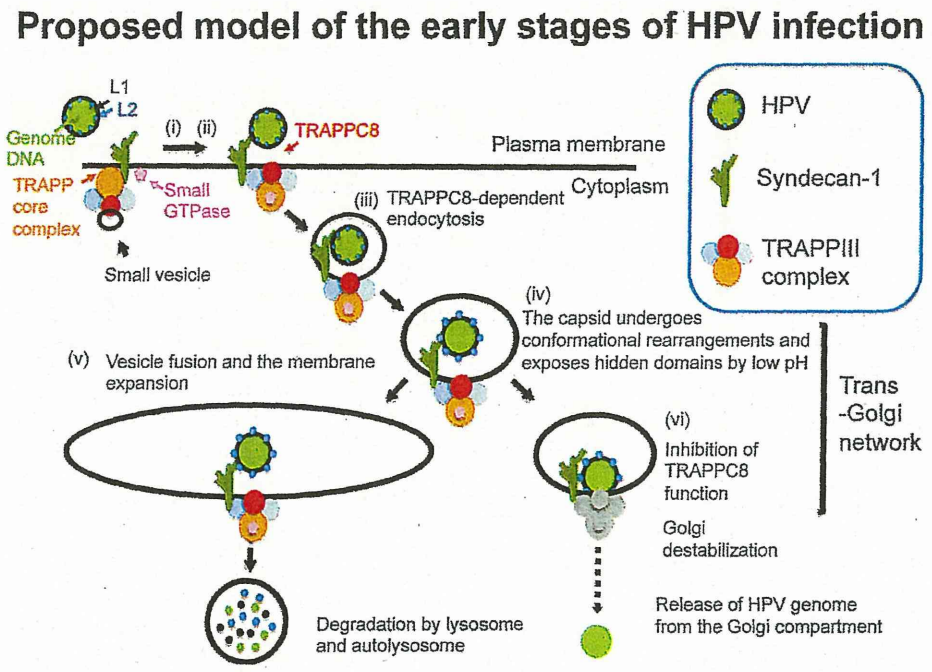

Figure 8. Proposed model for TRAPPC8 involvement in HPV infection. (i) HPV binds to HSPGs on the epithelial cell surface. (ii) The central region of TRAPPC8 is exposed on the cell surface upon virion attachment. (iii) The capsid is internalized into the cell by TRAPPC8-dependent endocytosis. (iv) The capsid undergoes conformational rearrangements and exposes hidden domains when exposed to low pH, leading to an exposure of the L2 N-terminal region. (v) Endosomal vesicles containing HPV51 Nu or HPV that fails to interact with TRAPPC8 are elongated or fused to each other, and these virions are eventually degraded by lysosomes and autolysosomes. (vi) HPV that interacts with TRAPPC8 through L2 inhibits TRAPPC8 functions, such as vesicle fusion and membrane expansion, both of which are necessary for the subsequent degradation process, thereby leading to the release of the viral genome from the trans-Golgi network.
doi:10.1371/journal.pone.0080297.g008

level of trypsin-resistant L1 was severely reduced in cells transfected with TRAPPC8 siRNA (KIAA1012-04). This result was reproduced in cells transfected with another TRAPPC8 siRNA (KIAA1012-03) (Figure S3A). In addition, we performed the same experiments using 51PsVNuL2, 51PsVL2–, 16PsV lacking L2 (16PsVL2–), and 31PsV lacking L2 (31PsVL2–) (Figure S2). As shown in Figure 4B, all PsVs exhibited reduced levels of trypsin-resistant L1 in TRAPPC8 knockdown cells when compared with cells transfected with control siRNA. These results indicate that TRAPPC8 plays a crucial role in PsV internalization, but that the process is independent of L2.

We further examined whether TRAPPC8 knockdown causes general defects in the endocytic uptake of non-HPV molecules like transferrin (Tf) and cholera toxin subunit B (CtxB). While Tf is internalized through dynamin-dependent, clathrin-mediated endocytosis [53], CtxB is internalized via both dynamin-dependent, clathrin- or caveolae-mediated endocytosis and dynamin-independent endocytosis [53,54]. TRAPPC8 knockdown in HeLa cells did not affect endocytic uptake of Tf (Figures 5A and 5C), suggesting that TRAPPC8 is not involved in dynamin-dependent, clathrin-mediated endocytosis. By contrast, transfection of TRAPPC8 siRNA caused partial defects in uptake of CtxB compared to control siRNA transfection (Figures 5B and 5C), implying that TRAPPC8 has a general role in either dynamin-independent or dynamin-dependent, caveolae-mediated endocytosis.

Subcellular localization of L1 and packaged DNA in cells inoculated with HPV51 PsVs

Because TRAPPC8 knockdown inhibited the internalization of PsVs in a manner independent of L2 interaction, we then investigated which stage of HPV infection requires L2-TRAPPC8 interaction. To this end, we monitored intracellular trafficking of 51PsVNuL2 or 51PsVMaL2 in the cell. HEK293FT cells were inoculated with these PsVs packaged with 5-ethynyl-2′-deoxyuridine (EdU)-labeled DNA. L1 and EdU-labeled DNA were visualized with the anti-51L1 antiserum and Click-it chemistry, respectively. In both 51PsVNuL2 and 51PsVMaL2-inoculated cells, EdU-labeled DNA and L1 colocalized (yellow dots, Figure 6A) on the cell surface at 0 h indicating cell attachment of the PsVs. After incubation for 8 h, EdU-labeled DNA (green dots, Figure 6A) was observed in the cytoplasm of 51PsVMaL2-inoculated cells, suggesting that PsV had been internalized and that its packaged DNA was separated from the L1 capsid (Figure 6A, right panel). In contrast, EdU-labeled DNA and L1 in the 51PsVNuL2-inoculated cells colocalized in the cytoplasm at 8 h. At 24 h, EdU-labeled DNA was transferred into the nucleus in 51PsVMaL2-inoculated cells, whereas EdU-labeled DNA and L1 in 51PsVMuL2-inoculated cells remained colocalized in the perinuclear region as large clusters without DNA translocation into the nucleus.

Since recent studies have revealed HPV trafficking to the trans-Golgi network (TGN) before genome translocation into the nucleus [33,34], we examined whether localization of EdU-

labeled DNA and L1 to the TGN differ between NuL2- and MaL2-containing PsVs. HEK293FT cells were inoculated with 51PsVNuL2 or 51PsVMaL2 and, after 8-h incubation, the TGN was visualized with anti-TGN46 antibody (trans-Golgi marker) together with staining of L1 and EdU-labled DNA. As shown in Figure 6B, while L1 staining was adjacent to or colocalized with the TGN similarly in both 51PsVNuL2 and 51PsVMaL2 (Figure 6B, upper panels, red dots), more EdU-labeled DNA signals were adjacent to the TGN in 51PsVMaL2-inoclated cells than in 51PsVNuL2-inoculated cells (Figure 6B, upper panels, green and yellow dots). Similar results were obtained by staining the cells with the Golgi marker, anti-GM130 antibody (Figure 6B, lower panels), suggesting that EdU-labeled DNA separated from L1 is more successfully localized in the Golgi in 51PsVMaL2-inoculated cells. These results raise the possibility that L2-TRAPPC8 interaction may be required for the viral genome localization in the TGN/Golgi compartment and that this L2 function could be related to the impaired infectivity observed in NuL2.

Golgi dispersal caused by L2 expression and TRAPPC8 knockdown

To further gain insight into roles for L2-TRAPPC8 interaction in the Golgi, we investigated Golgi morphology in cells expressing L2. HeLa cells were transfected with expression plasmids for a series of L2-GFP fusion proteins, and the Golgi bodies inside the cell visualized using anti-GM130 antibody. As shown in Figure 7, Golgi stacks were dispersed in the cells expressing MaL2-GFP, but not in the cells expressing NuL2-GFP. In contrast, immunofluorescence assays performed on cells expressing MaL2-GFP using the anti-early endosome antigen 1 (early endosome marker), anti-LAMP2 (late endosome marker) and anti-protein disulfide isomerase (ER marker) antibodies, did not reveal obvious structural changes in the corresponding organelles (Figure S4C). Golgi dispersal was also observed in cells expressing L2s that were capable of interacting with TRAPPC8, such as Ch5L2, HPV16 and HPV31 L2s (Figure 7, right panels). Intriguingly, TRAPPC8 knockdown in HeLa cells caused Golgi dispersal that was indistinguishable from that observed in MaL2-GFP expressing cells (Figure 7, left panels). Similarly, MaL2-GFP expression and TRAPPC8 knockdown did not affect early endosomes, late endosomes, or the ER (Figure S4A). Although we were unable to detect colocalization of PsV with TRAPPC8 in the Golgi compartment because of high anti-TRAPPC8 background staining of intracellular compartments (data not shown), these results suggest that the interaction between L2 and TRAPPC8 disrupts normal Golgi structure through inhibition of TRAPPC8 function.

Discussion

In this study we have identified TRAPPC8, a specific subunit of the mammalian TRAPPIII complex (mTRAPPIII), as an L2-interacting protein, and demonstrated that the knockdown of TRAPPC8 in human epithelial cells reduces both gene transduction with PsV and infectivity of authentic HPV virions. These observations strongly suggest that TRAPPC8 plays a central role in the early stages of HPV infection. However, TRAPPC8 knockdown inhibited the internalization of PsV independently of L2, thus excluding the requirement for L2-TRAPPC8 interaction during the initial entry step. Further, we find that the L2-TRAPPC8 interaction can induce Golgi dispersal and that this Golgi phenotype strongly correlates with the gene transduction efficiency of PsV. Thus, we propose two non-overlapping, L2-independent and -dependent roles for TRAPPC8 in the HPV cell entry mechanism.

For the L2-independent role of TRAPPC8, we propose a model in which the HPV virion, trapped by cell-surface L1-binding proteins such as HSPGs, is internalized by TRAPPC8-dependent endocytosis (Figure 8). The central region of TRAPPC8 was exposed on the surface of HeLa cells and colocalized with inoculated PsV (Figure 3B). These observations suggest the possibility that TRAPPC8 is located adjacent to HSPGs on the cell surface. Syndecans (syndecan-1 to -4) are a major class of membrane-spanning HSPGs, and their transmembrane (TM) and C-terminal cytosolic domains are highly conserved. Among the syndecans, syndecan-1 acts as an initial attachment protein for HPV entry into keratinocytes [55]. Given that TRAPPC4, one of the TRAPP core subunits, binds to the conserved EFYA motif at the C-terminus of syndecan-2 [56], it is possible that mTRAPPIII containing TRAPPC4 also binds to syndecan-1 in association with virion. Furthermore, TRAPPC8-containing vesicles beneath the plasma membrane may fuse with the plasma membrane trapping HPV, increasing exposure of its central region on the cell surface (Figure 3B). When considering the mechanism of TRAPPC8-dependent endocytosis, it is worth noting that TRAPP complexes regulate the function of small-GTPases via their GEF activity and by the combination of individual TRAPP subunits [43]. Thus, mTRAPPIII may regulate the GTPase activity of Rab5 and/or other unknown small GTPases that are necessary for the endocytosis of HPV [19,32].

TRAPPC8 knockdown did not affect uptake of transferrin (Figure 5), excluding the possibility that the effects of TRAPPC8 knockdown are non-specific and act on multiple endocytotic pathways. However, TRAPPC8 knockdown partially decreased uptake of cholera toxin, which is internalized via both dynamin-dependent and -independent endocytosis (Figure 5). Since TRAPPC8 knockdown reduces the cell's susceptibility to ricin [45], which enters the cell via a dynamin-independent pathway [54], and HPV also enters the host keratinocyte via a dynamin-independent pathway [19], TRAPPC8 may have a general role in this endocytotic pathway.

TRAPP complexes are involved in both the transport of vesicles from the ER to the Golgi and the endosome to the Golgi [43], and mTRAPPIII plays important roles in Golgi stack formation [47]. Recently, Day *et al.* and Lipovsky *et al.* reported that HPV16 is delivered to the TGN or the Golgi during the entry process [33,34], highlighting the importance of the TGN/Golgi compartment as a route for infectious HPV entry. Intriguingly, the Golgi dispersal phenotype observed in cells expressing L2s able to bind TRAPPC8 was almost identical to that seen in TRAPPC8 knockdown cells (Figures 7 and S4), suggesting that the interaction of L2 with TRAPPC8 inhibits its function in the Golgi. In contrast, L2s that can interact with TRAPPC8 did not affect early endosomes, late endosomes, or the ER (Figure S4C), which suggests a specific effect of L2-TRAPPC8 interaction on the Golgi structure. In summary, we speculate that the L2-TRAPPC8 interaction inhibits TRAPPC8 function in the Golgi and causes Golgi destabilization, thereby facilitating escape of the HPV genome from the Golgi compartment.

Since most regions in L2 molecules are buried in the capsid and the N-terminus of L2 becomes exposed on the capsid surface during the entry process [1,11], the L2 N-terminus including region I may interact with TRAPPC8 in the lumen of endocytotic vesicles. Although we were unable to detect direct interactions between recombinant TRAPPC8 and L2 (data not shown), TRAPPC12, another specific subunit contained in mTRAPPIII, showed similar L2-binding profiles to TRAPPC8 (Figure 1C, right

panel), suggesting that mTRAPPIII binds to L2 as an entire complex. Further support for this mechanism comes from the observation that the knockdown of TRAPPC12 in HeLa cells reduced susceptibility to gene transduction with 51MaL2PsV (Figure 2D). Similar results were obtained in HeLa cells transfected with siRNA against TRAPPC11, another subunit in mTRAPPIII (data not shown). These results suggest that mTRAPPIII as a whole plays an important role in HPV infection. In contrast, HeLa cells transfected with siRNA against TRAPPC9, one of the mTRAPPII subunits, exerted little or no effect on gene transduction with PsV (data not shown), suggesting that mTRAPPII is not involved in HPV infection. Moreover, the effects of siRNAs for each TRAPP subunit (TRAPPC8, 9, 11, and 12) on HPV infection show similar susceptibility to ricin, suggesting that HPV and ricin share the same entry pathway, a pathway that is dependent on mTRAPPIII.

Human TRAPPC8 has been shown to contribute to the autophagy system [46] and its yeast homolog, Trs85, is required for the formation of pre-autophagosomal structure and the membrane expansion of autophagosomes [43,44,57]. Thus the L2-TRAPPC8 interaction may lead to the arrests of vesicle fusion or membrane expansion at the TGN. These arrests are likely to protect HPV trapped in the lumen of the vesicle from subsequent degradation by lysosomes or autophagosomes. This model is further supported by recent findings that autophagy responses are induced in the initial stages of HPV16 infection [58], and that most internalized HPVs are degraded by autolysosomes [59,60]. We hypothesize that while most HPVs are degraded by the cell defense machinery, including the autophagy system, a proportion of internalized HPVs, i.e. those in which L2 binds to TRAPPC8, inhibit its function and thus escape from the TGN through Golgi destabilization (see Figure 8). NuL2, which lacks the capacity to bind to TRAPPC8, may not be able to avoid such degradation. Although further experiments are needed to substantiate our hypothetical models for the roles of TRAPPC8 in infectious HPV entry, our findings will contribute to a better understanding of the mechanisms by which HPV enters host cells and escapes from the TGN.

Supporting Information

Figure S1 Immunofluorescence microscopy analysis for TRAPPC8 on the cell surface. (A) Western blotting of lysates prepared from HeLa cells transfected with control or TRAPPC8 siRNA (KIAA1012-04) using anti-TRAPPC8 antibodies (anti-N1/603, anti-P880/894, and anti-P1270/1285). Upper panel: schematic diagram of TRAPPC8 and the peptides used for rabbit immunization. (B) HeLa cells were incubated with 51PsVMaL2 (MOI of ~2000 particles/cell) in growth medium at 4°C for 1 h. After washing with medium, the cells were incubated in medium with mouse anti-51L1 VLP antiserum and rabbit anti-N1/603 (left panel) or anti-P1270/1285 (right panel), followed by staining with Alexa Fluor 488-conjugated anti-mouse IgG and Alexa Fluor 546-conjugated anti-rabbit IgG. The cells were fixed and permeabilized, then mounted with Prolong Gold anti-fade reagent with DAPI. (C) HeLa cells were incubated with 51PsVMaL2 (MOI of ~2000 particles/cell) in growth medium at 4°C for 1 h. After removing unbound PsVs, the cells were incubated in medium with mouse anti-51L1 VLP antiserum and rabbit anit-P880/894, followed by staining with Alexa Fluor 488-conjugated anti-mouse IgG and Alexa Fluor 546-conjugated anti-rabbit IgG. The cells were fixed and permeabilized, then incubated with or without rabbit anti-N1/603, followed by staining with Alexa Fluor 647-conjugated goat anti-rabbit IgG. Fluorescence was visualized by confocal microscopy. The boxed areas are enlarged in the right panels. (D) Western blot analysis using commercial anti-TRAPPC8 antibody, sc-85191 (Santa Cruz Biotechnology Inc.). Truncated TRAPPC8 proteins, aa 1–603 (N1/603), aa 604–1435 (C604/1434), aa 604–747 (P604/747), aa 737–886 (P737/886), aa 876–1025 (P876/1025), aa 1015–1164 (P1015/1164), aa 1154–1303 (P1154/1303), and aa 1293–1435 (P1293/1435), were expressed in *E.coli* Rosetta-gami B (Takara Bio Inc.) by using the pCold II vector system (Takara Bio Inc.) and purified by nickel affinity chromatography. These proteins were electrophoresed and stained with CBB (upper panel). The proteins were analyzed by Western blotting using sc-85191 (lower panel). (E) Immunofluorescence microscopy analysis for cell-surface TRAPPC8 using sc-85191. HeLa cells were incubated with 51PsVMaL2 (MOI of ~2000 particles/cell) in growth medium at 4°C for 1 h. After removing unbound PsVs, the cells were incubated in medium with mouse anti-51L1 VLP antiserum and goat anti-TRAPPC8 antibody, sc-85191, followed by staining with Alexa Fluor 488-conjugated anti-mouse IgG and Alexa Fluor 546-conjugated anti-goat IgG. The cells were fixed and permeabilized, then incubated with rabbit anti-N1/603, followed by staining with Alexa Fluor 647-conjugated goat anti-rabbit IgG. Fluorescence was visualized by confocal microscopy. The boxed areas are enlarged in the right panels.
(TIF)

Figure S2 Characterization of PsVs. (A) Electrophoresis analysis of PsV fractions prepared from HEK293FT using the Opti-Prep gradient method as described in Materials and Methods. Proteins in the PsV fractions were stained with SYPRO Ruby. The arrows indicate the protein bands corresponding to L1 or L2. Right panel: molecule ratio between L1 and L2 in PsV fractions. (B) Electron micrograph of PsVs. The PsV fractions were settled on carbon-coated copper grids negatively stained with 2% uranyl acetate. The grids were examined using a Hitachi model H-7650 transmission electron microscope. (C) Ratio of DNase-resistant reporter plasmid to total reporter plasmid packaged in PsVs. PsV fractions were incubated with DNase-I, and DNase-resistant DNA was quantified by qPCR with the following primers complementary to the reporter plasmid pEF1α-EGFP: 5'-GCG GCC GCG CCA CCA TGG TGA GCA AGG GCG AGG AGC-3' and 5'-AAG CTT ACT TGT ACA GCT CGT CCA TGC CGA G-3'.
(TIF)

Figure S3 Effects of TRAPPC8 knockdown on PsV internalization. (A, B) HeLa cells transfected with control or TRAPPC8 siRNAs (KIAA1012-03 or -04) were inoculated with 51PsVMaL2, 51PsVNuL2, 51PsVL2–, 16PsV, 16PsVL2–, 31PsV, or 31PsVL2– (MOI of ~2000 particles/cell) and incubated for 1 h at 4°C. After washing with PBS, the cells were incubated in medium at 37°C for additional 0, 1, 2, 4 or 8 h. The cells were detached with PBS containing EDTA (Trypsin –) or PBS containing trypsin and EDTA (Trypsin +) at the indicated time points. The detached cells were lysed and boiled. Type 51L1, 16L1, 31L1, TRAPPC8, or α-tubulin were detected by Western blotting using anti-51MaL1 VLP antiserum, anti-HPV16L1 antibody (554171; BD Biosciences), anti-TRAPPC8 (anti-N1/603) and anti-α-tubulin antibodies, respectively. Asterisks: unknown protein that reacted with the anti-HPV16L1 antibody. Alpha-tubulin was detected as a loading control.
(TIF)

Figure S4 Effects of TRAPPC8 knockdown or 51MaL2 expression on intracellular organelles. (A) Effects of TRAPPC8 knockdown on early endosomes, late endosomes, or

the endoplasmic reticulum (ER). HeLa cells transfected with control or TRAPPC8 siRNA (KIAA1012-04) were incubated in medium at 37°C for 2 days. The cells were fixed, permeabilized, and incubated with anti-EEA1 (early endosome marker, 610457; BD Biosciences), anti-LAMP2 (late endosome marker, 555803; BD Biosciences) or anti-PDI (ER marker, ab2729; Abcam) antibody, followed by staining with Alexa Fluor 555-conjugated anti-mouse IgG, and mounted with Prolong Gold with DAPI. Fluorescence in the cells was examined by confocal microscopy. (B, C) Effects of expression of 51MaL2-GFP on early endosomes, late endosomes, or the ER. HeLa cells transfected with pCMV-GFP (B) or pCMV-51MaL2-GFP (C) were incubated in medium at 37°C for 24 h. The cells were fixed, permeabilized, and incubated with anti-GM130 (Golgi marker, 610822; BD Biosciences), anti-EEA1, anti-LAMP2, or anti-PDI antibody, followed by staining with Alexa Fluor 555-conjugated anti-mouse IgG, and mounted as described above. Fluorescence in the cells was examined by confocal microscopy. White arrows indicate cells expressing GFP or 51MaL2-GFP.
(TIF)

Acknowledgments

We thank Dr. Laimonis Laimins (Northwestern university) for kindly providing us with CIN612-9E cells. We are grateful to Dr. Tadahito Kanda for continuous encouragement of this work and Shiho Shimabukuro-Demoto for technical assistance.

Author Contributions

Conceived and designed the experiments: YI. Performed the experiments: YI TN. Analyzed the data: YI. Contributed reagents/materials/analysis tools: YI MK. Wrote the paper: YI IK TN RKM SM TT.

References

1. Buck CB, Cheng N, Thompson CD, Lowy DR, Steven AC, et al. (2008) Arrangement of L2 within the papillomavirus capsid. J Virol 82: 5190–5197.
2. de Villiers EM (2013) Cross-roads in the classification of papillomaviruses. Virology 445: 2–10.
3. Munoz N, Bosch FX, Castellsague X, Diaz M, de Sanjose S, et al. (2004) Against which human papillomavirus types shall we vaccinate and screen? The international perspective. Int J Cancer 111: 278–285.
4. Buck CB, Thompson CD, Roberts JN, Muller M, Lowy DR, et al. (2006) Carrageenan is a potent inhibitor of papillomavirus infection. PLoS Pathog 2: e69.
5. Combita AL, Touze A, Bousarghin L, Sizaret PY, Munoz N, et al. (2001) Gene transfer using human papillomavirus pseudovirions varies according to virus genotype and requires cell surface heparan sulfate. FEMS Microbiol Lett 204: 183–188.
6. Giroglou T, Florin L, Schafer F, Streeck RE, Sapp M (2001) Human papillomavirus infection requires cell surface heparan sulfate. J Virol 75: 1565–1570.
7. Johnson KM, Kines RC, Roberts JN, Lowy DR, Schiller JT, et al. (2009) Role of heparan sulfate in attachment to and infection of the murine female genital tract by human papillomavirus. J Virol 83: 2067–2074.
8. Joyce JG, Tung JS, Przysiecki CT, Cook JC, Lehman ED, et al. (1999) The L1 major capsid protein of human papillomavirus type 11 recombinant virus-like particles interacts with heparin and cell-surface glycosaminoglycans on human keratinocytes. J Biol Chem 274: 5810–5822.
9. Culp TD, Budgeon LR, Marinkovich MP, Meneguzzi G, Christensen ND (2006) Keratinocyte-secreted laminin 5 can function as a transient receptor for human papillomaviruses by binding virions and transferring them to adjacent cells. J Virol 80: 8940–8950.
10. Selinka HC, Giroglou T, Nowak T, Christensen ND, Sapp M (2003) Further evidence that papillomavirus capsids exist in two distinct conformations. J Virol 77: 12961–12967.
11. Richards RM, Lowy DR, Schiller JT, Day PM (2006) Cleavage of the papillomavirus minor capsid protein, L2, at a furin consensus site is necessary for infection. Proc Natl Acad Sci U S A 103: 1522–1527.
12. Day PM, Gambhira R, Roden RB, Lowy DR, Schiller JT (2008) Mechanisms of human papillomavirus type 16 neutralization by l2 cross-neutralizing and l1 type-specific antibodies. J Virol 82: 4638–4646.
13. Day PM, Lowy DR, Schiller JT (2003) Papillomaviruses infect cells via a clathrin-dependent pathway. Virology 307: 1–11.
14. Horvath CA, Boulet GA, Renoux VM, Delvenne PO, Bogers JP (2010) Mechanisms of cell entry by human papillomaviruses: an overview. Virol J 7: 11.
15. Laniosz V, Dabydeen SA, Havens MA, Meneses PI (2009) Human papillomavirus type 16 infection of human keratinocytes requires clathrin and caveolin-1 and is brefeldin a sensitive. J Virol 83: 8221–8232.
16. Raff AB, Woodham AW, Raff LM, Skeate JG, Yan L, et al. (2013) The Evolving Field of Human Papillomavirus Receptor Research: A Review of Binding and Entry. J Virol.
17. Sapp M, Bienkowska-Haba M (2009) Viral entry mechanisms: human papillomavirus and a long journey from extracellular matrix to the nucleus. FEBS J 276: 7206–7216.
18. Schelhaas M, Ewers H, Rajamaki ML, Day PM, Schiller JT, et al. (2008) Human papillomavirus type 16 entry: retrograde cell surface transport along actin-rich protrusions. PLoS Pathog 4: e1000148.
19. Schelhaas M, Shah B, Holzer M, Blattmann P, Kuhling L, et al. (2012) Entry of human papillomavirus type 16 by actin-dependent, clathrin- and lipid raft-independent endocytosis. PLoS Pathog 8: e1002657.
20. Schiller JT, Day PM, Kines RC (2010) Current understanding of the mechanism of HPV infection. Gynecol Oncol 118: S12–17.
21. Evander M, Frazer IH, Payne E, Qi YM, Hengst K, et al. (1997) Identification of the alpha6 integrin as a candidate receptor for papillomaviruses. J Virol 71: 2449–2456.
22. McMillan NA, Payne E, Frazer IH, Evander M (1999) Expression of the alpha6 integrin confers papillomavirus binding upon receptor-negative B-cells. Virology 261: 271–279.
23. Spoden G, Freitag K, Husmann M, Boller K, Sapp M, et al. (2008) Clathrin- and caveolin-independent entry of human papillomavirus type 16–involvement of tetraspanin-enriched microdomains (TEMs). PLoS One 3: e3313.
24. Scheffer KD, Gawlitza A, Spoden GA, Zhang XA, Lambert C, et al. (2013) Tetraspanin CD151 mediates papillomavirus type 16 endocytosis. J Virol 87: 3435–3446.
25. Woodham AW, Da Silva DM, Skeate JG, Raff AB, Ambroso MR, et al. (2012) The S100A10 subunit of the annexin A2 heterotetramer facilitates L2-mediated human papillomavirus infection. PLoS One 7: e43519.
26. Dziduszko A, Ozbun MA (2013) Annexin A2 and S100A10 Regulate Human Papillomavirus Type 16 Entry and Intracellular Trafficking in Human Keratinocytes. J Virol 87: 7502–7515.
27. Huang HS, Buck CB, Lambert PF (2010) Inhibition of gamma secretase blocks HPV infection. Virology 407: 391–396.
28. Karanam B, Peng S, Li T, Buck C, Day PM, et al. (2010) Papillomavirus infection requires gamma secretase. J Virol 84: 10661–10670.
29. Bienkowska-Haba M, Patel HD, Sapp M (2009) Target cell cyclophilins facilitate human papillomavirus type 16 infection. PLoS Pathog 5: e1000524.
30. Surviladze Z, Dziduszko A, Ozbun MA (2012) Essential roles for soluble virion-associated heparan sulfonated proteoglycans and growth factors in human papillomavirus infections. PLoS Pathog 8: e1002519.
31. Spoden G, Kuhling L, Cordes N, Frenzel B, Sapp M, et al. (2013) Human papillomavirus types 16, 18, and 31 share similar endocytic requirements for entry. J Virol 87: 7765–7773.
32. Smith JL, Campos SK, Wandinger-Ness A, Ozbun MA (2008) Caveolin-1-dependent infectious entry of human papillomavirus type 31 in human keratinocytes proceeds to the endosomal pathway for pH-dependent uncoating. J Virol 82: 9505–9512.
33. Day PM, Thompson CD, Schowalter RM, Lowy DR, Schiller JT (2013) Identification of a role for the trans-Golgi network in human papillomavirus 16 pseudovirus infection. J Virol 87: 3862–3870.
34. Lipovsky A, Popa A, Pimienta G, Wyler M, Bhan A, et al. (2013) Genome-wide siRNA screen identifies the retromer as a cellular entry factor for human papillomavirus. Proc Natl Acad Sci U S A 110: 7452–7457.
35. Bergant Marusic M, Ozbun MA, Campos SK, Myers MP, Banks L (2012) Human papillomavirus L2 facilitates viral escape from late endosomes via sorting nexin 17. Traffic 13: 455–467.
36. Bronnimann MP, Chapman JA, Park CK, Campos SK (2013) A transmembrane domain and GxxxG motifs within L2 are essential for papillomavirus infection. J Virol 87: 464–473.
37. Day PM, Baker CC, Lowy DR, Schiller JT (2004) Establishment of papillomavirus infection is enhanced by promyelocytic leukemia protein (PML) expression. Proc Natl Acad Sci U S A 101: 14252–14257.
38. Kamper N, Day PM, Nowak T, Selinka HC, Florin L, et al. (2006) A membrane-destabilizing peptide in capsid protein L2 is required for egress of papillomavirus genomes from endosomes. J Virol 80: 759–768.
39. Pereira R, Hitzeroth, II, Rybicki EP (2009) Insights into the role and function of L2, the minor capsid protein of papillomaviruses. Arch Virol 154: 187–197.
40. Bergant M, Banks L (2013) SNX17 facilitates infection with diverse papillomavirus types. J Virol 87: 1270–1273.
41. Wang JW, Roden RB (2013) L2, the minor capsid protein of papillomavirus. Virology.

42. Kondo K, Ishii Y, Mori S, Shimabukuro S, Yoshikawa H, et al. (2009) Nuclear location of minor capsid protein L2 is required for expression of a reporter plasmid packaged in HPV51 pseudovirions. Virology 394: 259–265.
43. Barrowman J, Bhandari D, Reinisch K, Ferro-Novick S (2010) TRAPP complexes in membrane traffic: convergence through a common Rab. Nat Rev Mol Cell Biol 11: 759–763.
44. Lynch-Day MA, Bhandari D, Menon S, Huang J, Cai H, et al. (2010) Trs85 directs a Ypt1 GEF, TRAPPIII, to the phagophore to promote autophagy. Proc Natl Acad Sci U S A 107: 7811–7816.
45. Bassik MC, Kampmann M, Lebbink RJ, Wang S, Hein MY, et al. (2013) A systematic mammalian genetic interaction map reveals pathways underlying ricin susceptibility. Cell 152: 909–922.
46. Behrends C, Sowa ME, Gygi SP, Harper JW (2010) Network organization of the human autophagy system. Nature 466: 68–76.
47. Scrivens PJ, Noueihed B, Shahrzad N, Hul S, Brunet S, et al. (2011) C4orf41 and TTC-15 are mammalian TRAPP components with a role at an early stage in ER-to-Golgi trafficking. Mol Biol Cell 22: 2083–2093.
48. Ishii Y, Tanaka K, Kondo K, Takeuchi T, Mori S, et al. (2010) Inhibition of nuclear entry of HPV16 pseudovirus-packaged DNA by an anti-HPV16 L2 neutralizing antibody. Virology 406: 181–188.
49. Kondo K, Ishii Y, Ochi H, Matsumoto T, Yoshikawa H, et al. (2007) Neutralization of HPV16, 18, 31, and 58 pseudovirions with antisera induced by immunizing rabbits with synthetic peptides representing segments of the HPV16 minor capsid protein L2 surface region. Virology 358: 266–272.
50. Ozbun MA, Meyers C (1997) Characterization of late gene transcripts expressed during vegetative replication of human papillomavirus type 31b. J Virol 71: 5161–5172.
51. Ozbun MA (2002) Human papillomavirus type 31b infection of human keratinocytes and the onset of early transcription. J Virol 76: 11291–11300.
52. Patterson NA, Smith JL, Ozbun MA (2005) Human papillomavirus type 31b infection of human keratinocytes does not require heparan sulfate. J Virol 79: 6838–6847.
53. Nonnenmacher M, Weber T (2011) Adeno-associated virus 2 infection requires endocytosis through the CLIC/GEEC pathway. Cell Host Microbe 10: 563–576.
54. Harper CB, Popoff MR, McCluskey A, Robinson PJ, Meunier FA (2013) Targeting membrane trafficking in infection prophylaxis: dynamin inhibitors. Trends Cell Biol 23: 90–101.
55. Shafti-Keramat S, Handisurya A, Kriehuber E, Meneguzzi G, Slupetzky K, et al. (2003) Different heparan sulfate proteoglycans serve as cellular receptors for human papillomaviruses. J Virol 77: 13125–13135.
56. Ethell IM, Hagihara K, Miura Y, Irie F, Yamaguchi Y (2000) Synbindin, A novel syndecan-2-binding protein in neuronal dendritic spines. J Cell Biol 151: 53–68.
57. Kakuta S, Yamamoto H, Negishi L, Kondo-Kakuta C, Hayashi N, et al. (2012) Atg9 vesicles recruit vesicle-tethering proteins Trs85 and Ypt1 to the autophagosome formation site. J Biol Chem 287: 44261–44269.
58. Surviladze Z, Sterk RT, DeHaro SA, Ozbun MA (2013) Cellular entry of human papillomavirus type 16 involves activation of the phosphatidylinositol 3-kinase/Akt/mTOR pathway and inhibition of autophagy. J Virol 87: 2508–2517.
59. Griffin LM, Cicchini L, Pyeon D (2013) Human papillomavirus infection is inhibited by host autophagy in primary human keratinocytes. Virology 437: 12–19.
60. Ishii Y (2013) Electron microscopic visualization of autophagosomes induced by infection of human papillomavirus pseudovirions. Biochem Biophys Res Commun 433: 385–389.

ANTICANCER RESEARCH *33*: 4995-4998 (2013)

Predicting Skin Toxicity According to *EGFR* Polymorphisms in Patients with Colorectal Cancer Receiving Antibody Against EGFR

RIE SAITO, HIDEO SUZUKI, TAKESHI YAMADA, SHINJI ENDO, TOSHIKAZU MORIWAKI, TAKUNORI UENO, MITSUAKI HIROSE, SACHIKO HIRAI, KENJI YAMATO, YUJI MIZOKAMI and ICHINOSUKE HYODO

Department of Gastroenterology, University of Tsukuba Graduate School, Tsukuba, Ibaraki, Japan

Abstract. *Background/Aim: Monoclonal antibodies against epidermal growth factor receptor (EGFR) can extend progression-free survival (PFS) and overall survival (OS) in patients with unresectable colorectal cancer; however, skin toxicity often interferes with therapy continuation. Patients and Methods: We analyzed the polymorphisms in EGFR and IgG fragment C receptor (FCGR) genes and determined their associations with clinical outcomes including PFS, OS, and skin toxicity. Five polymorphisms in EGFR and FCGR genes in 32 patients with unresectable colorectal cancer who were treated with antibodies against EGFR were examined. Results: Patients carrying the C/C genotype of the EGFR D994D polymorphism displayed significantly less skin toxicity than those with other genotypes, although no significant differences in PFS and OS were noted and no significant interactions were detected for other gene polymorphisms. Conclusion: These results suggest that the EGFR D994D polymorphism is a useful biomarker for predicting the severity of skin toxicity in patients receiving antibody against EGFR.*

Cetuximab and panitumumab are immunoglobulin G (IgG) antibodies against epidermal growth factor receptor (EGFR), and they have exhibited clinical activity both as monotherapies and in combination with chemotherapeutics in metastatic colorectal cancer (mCRC). The principal mechanism of action of these antibodies is based on the inhibition of ligand-induced *EGFR* activation, resulting in reduced cell proliferation, cell survival, and angiogenesis. In addition, cetuximab, and possibly panitumumab, may induce antibody-dependent cell cytotoxicity (ADCC) *via* the recruitment of cytotoxic host effector cells such as monocytes and natural killer cells (1, 2). The efficacy of ADCC may depend on the degree of activation of effector cells after IgG fragment C receptor (FCGR) IIa and IIIa engagement (3). The level of expression of *EGFR* in tumors has been considered a biomarker for the efficacy of therapy with antibody against EGFR; however, recent clinical studies revealed that the *v-Ki-ras2 Kirsten rat sarcoma viral oncogene homolog* (*KRAS*) status in tumors is the most useful biomarker to predict for efficacy of this therapy (4).

Although anti-EGFR therapy has greatly influenced the treatment of patients with mCRC, the therapy is associated with some side-effects that cannot be ignored. A major dose-limiting side-effect of anti-EGFR therapy is skin toxicity such as acne and paronychia, which often results in dose reduction or longer intervals between doses. The severity of acneiform skin rashes is associated with the efficacy of cetuximab (5), but as this adverse event occurs after therapy is initiated, it cannot be predicted before starting treatment. Several reports have shown an association of single nucleotide polymorphisms (SNPs) in *EGFR* and *FCGR* with clinical outcomes including therapeutic efficacy and side-effects (6, 7, 8), and some of these SNPs may be predictive biomarkers.

In this study, we investigated the influence of polymorphisms in *EGFR* and *FCGR* genes on the clinical response, skin toxicity, and survival of patients with mCRC who were treated with anti-EGFR, and identified genetic polymorphisms that may be useful biomarkers before treatment.

Patients and Methods

Patients and data collection. Thirty-two patients with unresectable recurrent CRC or mCRC who received chemotherapy including cetuximab (Bristol-Myers Squibb, NY, USA) or panitumumab (Takeda, Osaka, Japan) at the University of Tsukuba Hospital (Tsukuba, Ibaraki, Japan) were analyzed. The patients had histologically-confirmed CRC, and all patients had wild-type *KRAS*. Cetuximab or panitumumab was administered alone or in combination with chemotherapeutics such as 5-fluorouracil or irinotecan as a first-, second-, or third-line treatment between 2009 and 2012. Skin toxicity was evaluated by the National Cancer

Correspondence to: Hideo Suzuki, 1-1-1 Tennodai, Tsukuba, Ibaraki 305-8575, Japan. Tel: +81 298533218, Fax: +81 298533218, e-mail: hideoszk@md.tsukuba.ac.jp

Key Words: EGFR gene polymorphism, skin toxicity, colorectal cancer, EGFR antibody.

Institute Common Toxicity criteria (version 4.0)(http://evs.nci.nih.gov/ftp1/CTCAE/CTCAE_4.03_2010-06-14_QuickReference_5x7.pdf). The grade of skin toxicity at eight weeks after anti-EGFR administration was used for the evaluation. The tumor response to chemotherapy was evaluated by computed tomography every 2-3 months and defined according to the Response Evaluation Criteria in Solid Tumors (RECIST version 1.1) criteria (9) as complete response (CR), partial response (PR), stable disease (SD), or progressive disease (PD). Progression-free survival (PFS) and overall survival (OS) were calculated from the date of anti-EGFR administration to the date of progression and death, respectively. These data were retrospectively collected from the patients' medical records. This study was approved by the Institutional Review Board of the University of Tsukuba Hospital (#H21-483).

DNA extraction and genotyping. Genomic DNA was extracted from peripheral blood lymphocytes taken before anti-EGFR therapy using a Puregene Blood Core Kit (Qiagen, CA, USA). The *EGFR* polymorphisms analyzed in this study are shown in Table I. A Taqman 5' nuclease assay was performed using the ABI 7500 Sequence Detection System and SDS 2.3 software (Applied Biosystems, CA, USA) according to the manufacturer's protocol.

Statistical analysis. The interaction between polymorphisms in *EGFR* and *FCGR* genes and clinical outcomes was calculated by using Fisher's exact test. Comparisons of PFS according to genotype were performed using the Kaplan Meier method, and significance was determined using the log-rank test. Statistical analysis was conducted using SPSS 13.0 for Windows (IBM, NY, USA). Differences corresponding to $p<0.05$ were considered statistically significant.

Results

Patients' characteristics. The patients' demographics and genotype distribution are shown in Table II. All SNPs were amplified successfully in 91-100% of the samples. The genotypic frequency of each SNP was found to be in Hardy-Weinberg equilibrium (chi-square $p>0.05$). Patients were divided into two groups for each polymorphism of *EGFR* and *FCGR* genes such as C/C and C/T+T/T for the *EGFR D994D* SNP. There were no statistically significant differences in patients' characteristics between these groups.

Effects of genotype on clinical outcome and therapy-induced skin toxicity. As shown in Table III, there were no statistical differences in therapeutic response (CR+PR *vs.* SD+PD) according to polymorphisms in *EGFR* and *FCGR* genes. In addition, OS and PFS were not associated with any SNP in the examined genes (data not shown). The patients were divided into two groups according to the severity of skin rash as follows: grade 0-2 and grade 3. As shown in Table IV, the *EGFR D994D* C/C genotype was found to be significantly associated with less toxicity than the genotypes C/T and T/T ($p=0.038$). There were no significant differences in the response rate, PFS and OS between these genotypes (data not shown).

Table I. *SNPs evaluated*.

Gene	Location	Function	RS no.	Genotypic frequency	
				This study	Pacific Rim*
EGFR	5'-UTR		4444903	A/A=2 (6.3%)	16.7%
				A/G=13 (40.6%)	33.3%
				G/G=17 (53.1%)	50%
	Exon 13	R521K	2227983	A/A=12 (37.5%)	
				A/G=16 (50%)	
				G/G=4 (12.5%)	
	Exon 25	D994D	2293347	C/C=13 (40.6%)	45.8%
				C/T=16 (50%)	45.8%
				T/T=3 (9.4%)	8.3%
FCGRIIa	Exon 4	H166R	1801274	A/A=1 (3.4%)	50%
				A/G=17 (58.6%)	41.7%
				G/G=11 (38%)	8.3%
FCGRIIIa	Exon 5	F212V	396991	C/C=19 (61.3%)	8.3%
				C/A=11 (35.5%)	87.5%
				A/A=1 (3.2%)	4.2%

*The reported genotypic frequency (Pacific Rim) was obtained from the National Cancer Institute SNP500 cancer website (http://variantgps.nci.nih.gov/cgfseq/pages/snp500.do).

Discussion

Previous reports revealed a relationship between *EGFR* gene polymorphisms and clinical status. Graziano *et al.* reported that anti-EGFR-treated patients with fewer *EGFR* intron 1 and *EGF* 61 G/G genotypes experienced longer survival (10). Bibeau *et al.* reported that the *FCGR* IIIa polymorphism is associated with better PFS in patients with mCRC treated with cetuximab (7). In our study, although the number of patients may not be sufficient, polymorphisms in *EGFR* and *FCGR* genes did not display any significant associations with response to anti-EGFR therapy, and no significant effect of these polymorphisms on PFS and OS was detected. The relationship between polymorphisms in *EGFR* and *FCGR* genes and therapy-derived clinical outcome remains controversial. Concerning skin toxicity, Graziano *et al.* reported that EGFR intron-1 S/S carriers more frequently exhibited serious skin toxicity than L/L carriers (10). By contrast, Klinghammer *et al.* identified the *EGFR R521K* SNP but not the *EGFR* intron-1 CA repeats polymorphism as an attractive predictor of the occurrence of skin-related side-effects (8). Although only the *EGFR D994D* SNP was found to be related to skin toxicity in this study, the effect of this SNP on clinical outcome is controversial. Ma *et al.* reported that the *EGFR D994D* SNP is a predictive biomarker in patients with advanced non-small cell lung cancer treated with gefitinib (11). On the contrary, Shitara *et al.* reported that the EGFR 8227 G/A polymorphism, but not the *EGFR D994D* polymorphism, might be associated with clinical outcome in

Table II. *Patient characteristics and distribution by genotype (n=32).*

Factor	n	%	*EGFR* 5'-UTR 61A>G			*EGFR* R521K			*EGFR* D994D			*FCGRIIa* 131G>A			*FCGRIIIa* 158 T>G		
			A/A+ A/G	G/G	*p*-Value	A/A	A/G+ G/G	*p*-Value	C/C	C/T+ T/T	*p*-Value	A/A+ A/G	G/G	*p*-Value	C/C	C/A+ A/A	*p*-Value
Gender					0.6			0.85			0.78			0.6			0.58
Male	21	65.6	10	11		7	14		8	13		11	7		12	8	
Female	11	34.4	5	6		5	6		5	6		7	4		7	4	
Age.years																	
Median (range)	61	(34-84)	60±10	58±13	0.61	64±13	56±10	0.09	60±8	58±12	0.76	57±10	63±14	0.24	61±13	55±8	0.18
ECOG PS					0.81			0.17			0.91			0.43			0.89
0	21	65.6	9	12		7	14		8	13		11	10		8	12	
1	9	28.1	5	4		3	6		4	5		5	4		3	6	
2	2	6.3	1	1		2	0		1	1		2	0		1	1	
Therapy					0.34			0.68			0.46			0.2			0.94
CPT11+cetuximab	8	25	6	2		2	6		4	4		3	5		4	4	
Cetuximab	3	9.4	1	2		2	1		2	1		1	2		1	2	
FOLFOX+panitumumab	3	9.4	1	2		2	1		0	3		3	0		1	2	
FOLFIRI+panitumumab	9	28.1	3	6		3	6		4	5		6	1		2	6	
CPT11+panitumumab	2	6.2	0	2		1	1		0	2		1	0		1	1	
Panitumumab	7	21.9	4	3		2	5		3	4		4	3		3	4	
Therapy line					0.57			0.71			0.51			0.52			0.88
First	3	9.4	1	2		2	1		0	3		3	0		1	2	
Second	11	34.4	4	7		4	7		5	6		5	4		4	7	
Third	14	43.7	7	7		5	9		6	8		8	5		6	7	
Fourth	4	12.5	3	1		1	3		2	2		2	2		1	3	

ECOG, Eastern Cooperative Oncology Group; FOLFOX, 5-fluorouracil, leucovorin, and oxaliplatin; FOLFIRI, 5-fluorouracil, leucovorin, and irinotecan; CPT-11, camptothecin 11.

Table III. *Response rate by genotype.*

	EGFR 5'-UTR 61A>G		*EGFR* R521K		*EGFR* D994D		*FCGRIIa* 131G>A		*FCGRIIIa* 158 T>G	
Response	A/A,A/G	G/G	A/A	A/G,G/G	C/C	C/T,T/T	A/A,A/G	G/G	C/C	C/A,A/A
CR,PR	3	6	3	6	5	4	6	3	6	2
SD,PD	12	11	9	14	8	15	12	8	13	10
p-Value*	0.287		0.546		0.248		0.534		0.313	

*Fisher's exact test. CR, Complete Response; PR, Partial Response; SD, Stable Disease; PD, Progressive Disease.

Table IV. *Skin.toxicity by genotype.*

	EGFRV-VTR 61A>G		*EGFR* R521K		*EGFR* D994D		*FCGRIIa* 131G>A		*FCGRIIIa* 158 T>G	
Grade	A/A,A/G	G/G	A/A	A/G,G/G	C/C	C/T,T/T	A/A,A/G	G/G	C/C	C/A,A/A
0,1,2	11	12	9	14	12	11	12	10	14	8
3	4	5	3	6	1	8	6	1	5	4
p-Value*	0.589		0.546		0.038		0.151		0.489	

*Fisher's exact test. The skin toxicity grade was scored from 0 to 3 according to National Cancer Institute Common Toxicity Criteria (version 4.0) (httpV/evs.nci.nih.gov/ftp 1/CTCAE/CTCAE_4.03_2010-06- 14_QuickReference_5×7.pdf).

EGFR tyrosine kinase inhibitor-treated patients with non-small cell lung cancer (12). There is no report describing an association between the *EGFR D994D* polymorphism and skin toxicity in patients treated with anti-EGFR antibodies. Although the *EGFR D994D* SNP is synonymous and considered not to change the amino acid sequence of the protein nor affect the biological function of the protein itself, the SNP may have functional significance because it is located in the coding region in exon 25 of the *EGFR* gene (11). Indeed, recent studies revealed it affected the stability, splicing and the translational kinetics of the mRNA, resulting in changes in the amount, structure and function of proteins (13-15). Further research at the molecular level is expected to clarify the influence of this SNP on biological functions.

There are some limitations to this study. Firstly, our findings were obtained from a relatively small number of patients. Secondly, we examined only five polymorphisms of genes within the *EGFR* pathway. Thirdly, there is therapeutic bias for the clinical outcome because different chemotherapies were used and two antibodies against EGFR, cetuximab and panitumumab, were regarded as a single therapy.

In conclusion, the *EGFR D994D* polymorphism is a candidate biomarker to predict for severity of skin toxicity in patients receiving anti-EGFR therapy. As the detailed functions of this SNP are unknown, larger sample sizes and further investigations at the molecular level are required.

Conflicts of Interest

None.

Acknowledgements

We would like to thank Dr. Takako Nakamura for technical advice concerning genotyping. This study was funded by the Ministry of Health, Labor and Welfare, Japan (grant no. 21790140).

References

1 Ciardiello F and Tortora G: EGFR antagonists in cancer treatment. N Engl J Med *358*: 1160-1174, 2008.

2 Iannello A and Ahmad A: Role of antibody-dependent cell-mediated cytotoxicity in the efficacy of therapeutic anticancer monoclonal antibodies. Cancer Metastasis Rev *24*: 487-499, 2005.

3 Kurai J, Chikumi H, Hashimoto K, Yamaguchi K, Yamasaki A, Sako T, Touge H, Makino H, Takata M, Miyata M, Nakamoto M, Burioka N and Shimizu E: Antibody-dependent cellular cytotoxicity mediated by cetuximab against lung cancer cell lines. Clin Cancer Res *13*: 1552-1561, 2007.

4 Lievre A, Bachet JB, Boige V, Cayre A, Le Corre D, Buc E, Ychou M, Bouché O, Landi B, Louvet C, André T, Bibeau F, Diebold MD, Rougier P, Ducreux M, Tomasic G, Emile JF, Penault-Llorca F and Laurent-Puig P: *KRAS* mutations as an independent prognostic factor in patients with advanced colorectal cancer treated with cetuximab. J Clin Oncol *26*: 374-379, 2008.

5 Jonker DJ, O'Callaghan CJ, Karapetis CS, Zalcberg JR, Tu D, Au HJ, Berry SR, Krahn M, Price T, Simes RJ, Tebbutt NC, van Hazel G, Wierzbicki R, Langer C and Moore MJ: Cetuximab for the treatment of colorectal cancer. N Engl J Med *357*: 2040-2048, 2007.

6 Zhang W, Gordon M, Press OA, Rhodes K, Vallböhmer D, Yang DY, Park D, Fazzone W, Schultheis A, Sherrod AE, Iqbal S, Groshen S and Lenz HJ: Cyclin D1 and epidermal growth factor polymorphisms associated with survival in patients with advanced colorectal cancer treated with cetuximab. Pharmacogenet Genomics *16*: 475-483, 2006.

7 Bibeau F, Lopez-Crapez E, Di Fiore F, Thezenas S, Ychou M, Blanchard F, Lamy A, Penault-Llorca F, Frébourg T, Michel P, Sabourin JC and Boissière-Michot F: Impact of FccRIIa–FccRIIIa polymorphisms and *KRAS* mutations on the clinical outcome of patients with metastatic colorectal cancer treated with cetuximab plus irinotecan. J Clin Oncol *27*: 1122-1129, 2009.

8 Klinghammer K, Knödler M, Schmittel A, Budach V, Keilholz U and Tinhofer I: Association of *EGFR* polymorphism, skin toxicity, and outcome in patients with squamous cell carcinoma of the head and neck receiving cetuximab-docetaxel treatment. Clin Cancer Res *16*: 304-310, 2010.

9 Eisenhauer EA, Therasse P, Bogaerts J, Schwartz LH, Sargent D, Ford R, Dancey J, Arbuck S, Gwyther S, Mooney M, Rubinstein L, Shankar L, Dodd L, Kaplan R, Lacombe D and Verweij J: New response evaluation criteria in solid tumours: revised RECIST guideline (version 1.1). Eur J Cancer *45*: 228-47, 2009.

10 Graziano F, Ruzzo A, Loupakis F, Canestrari E, Santini D, Catalano V, Bisonni R, Torresi U, Floriani I, Schiavon G, Andreoni F, Maltese P, Rulli E, Humar B, Falcone A, Giustini L, Tonini G, Fontana A, Masi G and Magnani M: Pharmacogenetic profiling for cetuximab plus irinotecan therapy in patients with refractory advanced colorectal cancer. J Clin Oncol *26*: 1427-1434, 2008.

11 Ma F, Sun T, Shi Y, Yu D, Tan W, Yang M, Wu C, Chu D, Sun Y, Xu B and Lin D: Polymorphisms of *EGFR* predict clinical outcome in advanced non-small cell lung cancer patients treated with gefitinib. Lung Cancer *66*: 114-119, 2009.

12 Shitara M, Sasaki H, Yokota K, Okuda K, Hikosaka Y, Moriyama S, Yano M, Kawaguchi T, Kubo A, Takada M, Kitahara N, Okumura M, Matsumura A, Iuchi K and Fujii Y: Polymorphisms in intron 1 of the *EGFR* gene in non-small cell lung cancer patients. Exp Ther Med *4*: 785-789, 2012.

13 Sauna ZE, Kimchi-Sarfaty C, Ambudkar SV and Gottesman MM: Silent polymorphisms speak: How they affect pharmacogenomics and the treatment of cancer. Cancer Res *67*: 9609-9612, 2007.

14 Nackley AG, Shabalina SA, Tchivileva IE, Satterfield K, Korchynskyi O, Makarov SS, Maixner W and Diatchenko L: Human catechol-*O*-methyltransferase haplotypes modulate protein expression by altering mRNA secondary structure. Science *314*: 1930-1933, 2006.

15 Capon F, Allen MH, Ameen M, Burden AD, Tillman D, Barker JN and Trembath RC: A synonymous SNP of the corneodesmosin gene leads to increased mRNA stability and demonstrates association with psoriasis across diverse ethnic groups Hum Mol Genet *13*: 2361-2368, 2004.

Received July 23, 2013
Revised September 27, 2013
Accepted September 30, 2013

Oncology Research, Vol. 21, pp. 155–164

0965-0407/14 $90.00 + .00
DOI: http://dx.doi.org/10.3727/096504013X13854886566598
E-ISSN 1555-3906
www.cognizantcommunication.com

The Sirtuin Inhibitor Tenovin-6 Upregulates Death Receptor 5 and Enhances Cytotoxic Effects of 5-Fluorouracil and Oxaliplatin in Colon Cancer Cells

Takunori Ueno, Shinji Endo, Rie Saito, Mitsuaki Hirose,
Sachiko Hirai, Hideo Suzuki, Kenji Yamato, and Ichinosuke Hyodo

Department of Gastroenterology, University of Tsukuba Graduate School, Tsukuba, Ibaraki, Japan

It has been reported that upregulated SIRT1 (NAD^+-dependent class III histone deacetylase) deacetylates the p53 protein, represses its function, and allows for tumor cell growth in various cancers. Here we investigated antitumor effects of tenovin-6, a small-molecule inhibitor of SIRT1 and SIRT2, in various colon cancer cell lines. Tenovin-6 induced apoptosis in all five colon cancer cell lines investigated (two cell lines with wild-type *p53* and three with mutant *p53*) regardless of the *p53* mutation status. This effect was accompanied by accumulation of death receptor 5 (DR5) in most cell lines. DR5 silencing in HCT116 cells strongly attenuated tenovin-6-induced apoptosis. We investigated the effect of combining tenovin-6 with conventional anticancer agents 5-fluorouracil (5-FU), SN-38 (an active metabolite of irinotecan), and oxaliplatin. Synergistic antitumor effects of tenovin-6 were observed in combination with either 5-FU or oxaliplatin in vitro. The combination of tenovin-6 and oxaliplatin exhibited potent growth inhibition of HCT116 xenograft tumors in vivo. In conclusion, tenovin-6 induced apoptosis in human colon cancer cells through the activation of the DR5 signaling pathway and enhanced the antitumor properties of 5-FU and oxaliplatin. These results may help develop a novel treatment option for colorectal cancer using a SIRT inhibitor.

Key words: Tenovin-6; Colorectal cancer; Sirtuin 1 (SIRT1); Sirtuin 2 (SIRT2); Death receptor 5 (DR5); Cancer therapy

INTRODUCTION

Inactivation of p53 pathways is one of the most common alterations during human carcinogenesis (1–3). A loss-of-function mutation or deletion of the *p53* tumor-suppressor gene is reported in approximately half of human cancer cases. In other tumors, the function of intact p53 is often inhibited by various mutations and modifications in its pathway. Sirtuin 1 (SIRT1), a nicotinamide adenine dinucleotide (NAD^+)-dependent class III histone deacetylase (HDAC), is involved in chromatin silencing and regulation of life span and genomic stability (4–6). It plays an important role in cell survival under genotoxic and oxidative stress via deacetylation of key cell cycle molecules and apoptosis-regulatory proteins including p53, forkhead box (FOXO) family proteins, nuclear factor κB, and Ku70 (7–9). Acetylation of p53 is one of the important posttranslational modifications to activate the p53 signaling pathway as well as phosphorylation (10,11). Deacetylation of p53 suppresses its activity as a transcription factor toward its target genes that drive cell cycle arrest and apoptosis. Overexpression of SIRT1 has been found in some types of cancer including colorectal cancer (8,9,12–14) and has been suspected of promoting tumor progression. SIRT2 is a homologous deacetylase, which acts on receptor-interacting protein 1 (RIP1) and regulates the programmed cell necrosis (15). SIRT2 deacetylates α-tubulin and partly regulates cell mobility (16). The function of SIRT2 in carcinogenesis and cancer progression has not been fully elucidated yet.

Much attention is now focused on tenovin-6 (Fig. 1) as one of the agents that demonstrate antitumor effect by activating p53 (17–20). Lain et al. carried out a cell-based screen of 30,000 drug-like small molecules for their ability to activate p53. This cell-based screen identified tenovin-1 (Fig. 1), which act as an activator of p53. Tenovin-6 is a water-soluble analog of tenovin-1. Through the target-finding studies of tenovins, they revealed that tenovin-6 specifically inhibited purified mammalian SIRT1 and SIRT2 peptide deacetylase activity in vitro (17,18). It suppresses tumor growth in vitro at single-digit micromolar concentrations and delays tumor growth of a human melanoma xenograft in vivo without significant toxicity (18). In addition, tenovin-6 has been reported to exert antitumor effect against not only cancer cells with wild-type (wt) *p53* but also those with a *p53* null or mutant (mt) *p53* (18); these data are suggestive

Address correspondence to Shinji Endo, Department of Gastroenterology, University of Tsukuba Graduate School, 1-1-1 Tennodai, Tsukuba, Ibaraki 305-8575, Japan. Tel/Fax: +81-29-853-3218; E-mail: shinj.endo@md.tsukuba.ac.jp

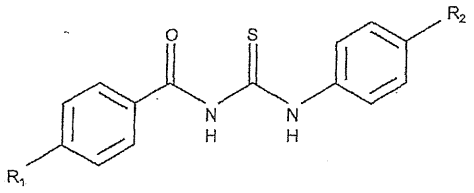

	R_1	R_2
tenovin-1	^{t}Bu	$NHCOCH_3$
tenovin-6	^{t}Bu	$NHCO(CH_2)_4NMe_2.HCl$

Figure 1. Chemical structure of tenovin-1 and tenovin-6.

of the influence of tenovin-6 on *p53*-independent tumor-suppressive pathways.

The signaling pathways of apoptosis are classified as intrinsic and extrinsic. Death receptor 5 (DR5) is one of TNF-related apoptosis-inducing ligand (TRAIL) receptors in the extrinsic apoptotic pathway. To date, several reports have suggested that some histone deacetylase inhibitors upregulate DR5, leading to apoptosis (21–26). To explore this possibility, we examined if tenovin-6 induced apoptosis via the DR5 pathway in various colon cancer cell lines. Furthermore, we tried to identify the best combination of tenovin-6 with standard drugs for the treatment of metastatic colorectal cancer such as 5-fluorouracil (5-FU), oxaliplatin, and SN-38 (a major active metabolite of irinotecan) in vitro and in vivo.

MATERIALS AND METHODS

Chemicals

Tenovin-6 was purchased from Cayman Chemical (Ann Arbor, MI, USA) and dissolved in dimethyl sulfoxide (DMSO) at a concentration of 20 mM; aliquots were stored at –20°C. Stock solutions were diluted to the desired final concentrations with growth medium prior to use. Oxaliplatin, SN-38, and 5-FU were purchased from Wako (Osaka, Japan) and Sigma–Aldrich (St. Louis, MO, USA).

Cell Lines and Cell Culture

Human colon cancer cell lines with (wild-type) wt-*p53* (HCT116 and LoVo) and (mutant) mt-*p53* (DLD-1, HT29, and CaCo2) were purchased from American Type Culture Collection (Rockville, MD, USA). Normal human fibroblast MRC5 cell line was obtained from RIKEN BRC cell Bank (Japan). Cell lines were cultured in the following media: HCT116 cells and HT29 cells in McCoy's 5A medium (Sigma–Aldrich) with 10% fetal bovine serum (FBS; Nichirei Biosciences, Tokyo, Japan), LoVo cells in Ham's F12K medium (Invitrogen, Carlsbad, CA, USA) with 10% FBS, DLD-1 cells in the RPMI 1640 medium (Sigma–Aldrich) with 10% FBS, CaCo2 cells in Eagle's minimum essential medium (Sigma–Aldrich) with 20% FBS, and MRC5 cells in MEMα (WAKO, Osaka, Japan) with 10% FBS.

The Cell Viability Assay

Cells in 96-well cell culture plates were treated with vehicle (DMSO) alone, single agents or combinations at indicated doses. After 72 h incubation, WST-8 colorimetric assays were performed as previously described using the Cell Counting Kit-8 (Dojin Laboratories Kumamoto, Japan) and an iMark microplate reader (Bio-Rad, Hercules, CA, USA) (27).

Real-Time Quantitative PCR Analysis of SIRT1 and SIRT2 Expression

Total RNA was extracted using the High Pure RNA Isolation kit (Roche Diagnostics, Mannheim, Germany), and cDNA was synthesized with High Capacity RNA-to-cDNA kit (Life Technologies Corp., Carlsbad, CA, USA). *SIRT1* and *SIRT2* mRNA expressions were analyzed on an Applied Biosystems 7500 Fast Real-Time PCR System (Applied Biosystems, Foster City, CA, USA). Primers and a TaqMan probe for *SIRT1* and *SIRT2* were purchased from Applied Biosystems, and those for 18S ribosomal RNA (18S rRNA) were designed and synthesized by Sigma–Aldrich Corp. The sequence of the 18S rRNA-specific oligonucleotides was as follows: 5′-AACCCGTTGAACCCCATTCG (forward primer), 5′-CGGGCGGTGTGTACAAAGG (reverse primer), and 5′-AACGCAAGCTTATGACCCGCACTTACTGG (probe). Reactions were performed in triplicate under standard thermocycling conditions using 30 ng cDNA, 900 nM primers, 250 nM of the probe, and a TaqMan Gene Expression Master Mix (Applied Biosystems), according to the manufacturer's protocol.

Western Blotting

Cells were lysed on ice with RIPA buffer (WAKO). Protein concentrations were determined using Bio-Rad DC Protein Assay Reagent and iMark microplate absorbance reader (Bio-Rad). The proteins in the samples were separated using SDS-PAGE and blotted onto PVDF membranes as described previously (27). The protein bands were detected using the ECL prime Western Blotting Detection system (GE Healthcare Life Sciences, Buckinghamshire, UK), according to the manufacturer's protocol. The signal intensity was quantified using Ez-capture II chemiluminescence imaging system (Atto, Tokyo, Japan).

Western blotting was performed using the following antibodies: anti-SIRT1 (D739), anti-acetylated (Ac)-p53 (Lys382), anti-DR5, anticleaved poly(ADP)-ribose polymerase {PARP} (Asp214), anticleaved caspase-3 (Asp175), mouse anti-$p21^{Waf/Cip1}$ (DCS60), and anti-β-actin

(8H10D10) antibodies were purchased from Cell Signaling Technology (Danvers, MA, USA). Anti-p53 (BP53-12) and anti-SIRT2 (4B11) antibodies were obtained from Cell Science (Canton, MA, USA) and Sigma–Aldrich Corp, respectively. Conjugated anti-mouse IgG sheep and anti-rabbit IgG donkey sera were obtained from GE Healthcare Life Sciences.

Transfection With Small Interfering RNA (siRNA) Against DR5

Cells were seeded in 6- or 96-well plates. The following day, the cells were transfected with either siRNA against DR5 or with control siRNA at the concentration of 1 nM. The sense and antisense strands of DR5 siRNA are CCGUUUGUGCGUACUUUGAGA (sense) and UCAAAGUACGCACAAACGGAA (antisense). Those of control siRNA are CCGUACUAGCCAUUAUGCGUC (sense) and CGCAUAAUGGCUAGUACGGGU (anti sense). SiRNAs were designed using the siDirect software (http://sidirect2.rnai.jp/) as described previously (28). The siRNA transfection was performed using Lipofectamine RNAiMAX (Invitrogen) according to the manufacturer's instructions.

Flow Cytometry

Cells were seeded in 60-mm dishes at a density of 2×10^5 cells per dish. After incubation with tenovin-6 (10 μM) or an equivalent amount of DMSO for 72 h, the cells were gently harvested with Accutase (US Biotechnologies, Parker Ford, PA, USA) at room temperature for 10 min. Apoptotic cells were detected using double staining with propidium iodide (PI) and fluorescein isothiocyanate (FITC)-labeled annexin V using an annexin V–FITC Apoptosis Detection Kit (Beckman Coulter, Brea, CA, USA), according to the manufacturer's protocol. Flow cytometry was then performed on a FACS Calibur flow cytometer (BD Biosciences, NJ, USA) and CELL Quest software (BD Biosciences).

Animal and Xenograft Colon Cancer Model

Six-week-old female nude mice (BALB/c nu/nu) were purchased from Charles River Japan (Kanagawa, Japan) and maintained under special pathogen-free conditions in a temperature- and humidity-controlled environment. A xenograft colon cancer model consisted of injection of HCT116 cells (5×10^6 cells) in 100 μl of Hank's balanced salt solution (Sigma–Aldrich) subcutaneously into the right side of the back of the animals.

Tumor volumes were calculated every other day using the following equation: volume = length × width^2 × 0.52. At tumor volume of approximately 100 mm^3, the mice were randomly distributed into four groups ($n=6$) as follows: tenovin-6 alone, oxaliplatin alone, tenovin-6 plus oxaliplatin, and control (DMSO). Treatment was started on the same day of initial randomization. Tenovin-6 and oxaliplatin were injected on days 9 and 17. Additional tenovin-6 was administered on day 11. Each chemotherapeutic regimen was administered via 400-μl intraperitoneal injections at the following concentrations: tenovin-6 30 mg/kg and oxaliplatin 5 mg/kg. To monitor health, the mice were weighed every 2 days, and their general physical condition was recorded daily. The Institutional Animal Care and Use Committee of the University of Tsukuba approved all the experimental protocols (Permit number: 106).

Combination Index

To test if tenovin-6 can enhance antitumor effects of the chemotherapeutic agents, we determined a combination index (CI) and built an isobologram using the CalcuSyn software (Cambridge, UK), according to the Chou and Talalay median effect principle (29). In this analysis, CI > 1.3 indicates antagonism, CI = 1.1–1.3 moderate antagonism, CI = 0.9–1.1 additive effect, CI = 0.8–0.9 slight synergism, CI = 0.6–0.8 moderate synergism, CI = 0.4–0.6 synergism, and CI = 0.2–0.4 strong synergism.

Statistical Analysis

All data were expressed as the mean ± standard deviation (SD). Statistical difference was determined by Student's t test. Two-sided values of $p<0.05$ were assumed to indicate statistical significance.

RESULTS

Expression Levels of SIRT1 and SIRT2 in Colon Cancer Cells

SIRT1 and SIRT2 protein expression were evaluated in a panel of five human colon cancer cell lines [two cell lines with wt-*p53* (HCT116 and LoVo) and three cell lines with mt-*p53* (DLD-1, HT29, and CaCo2)] by Western blotting (Fig. 2a). The levels of mRNA expression of *SIRT1* and *SIRT2* were estimated by qRT-PCR (Fig. 2b). The expression of SIRT1 was upregulated in all cancer cell lines, whereas the levels of SIRT2 protein and mRNA were not significantly different among the five cancer cell lines and normal fibroblast MRC5 cells. SIRT1 protein expression in CaCo2 cells was threefold higher, and *SIRT1* mRNA expression was fivefold higher compared with MRC5 cells.

Tenovin-6 Inhibited Cell Growth and Induced Apoptosis in Colon Cancer Cells

To evaluate the antitumor activity of tenovin-6 on colon cancer, five colon cancer cell lines were exposed to various concentrations of tenovin-6 (0, 0.2, 1, 5, 10, and 20 μM) for 72 h and tested for viability. Tenovin-6 showed strong cell growth inhibition with IC_{50} ranging from 1.26 to 2.58 μM in those cell lines except CaCo2 cells, whose IC_{50} was 8.21 μM (Fig. 3a).

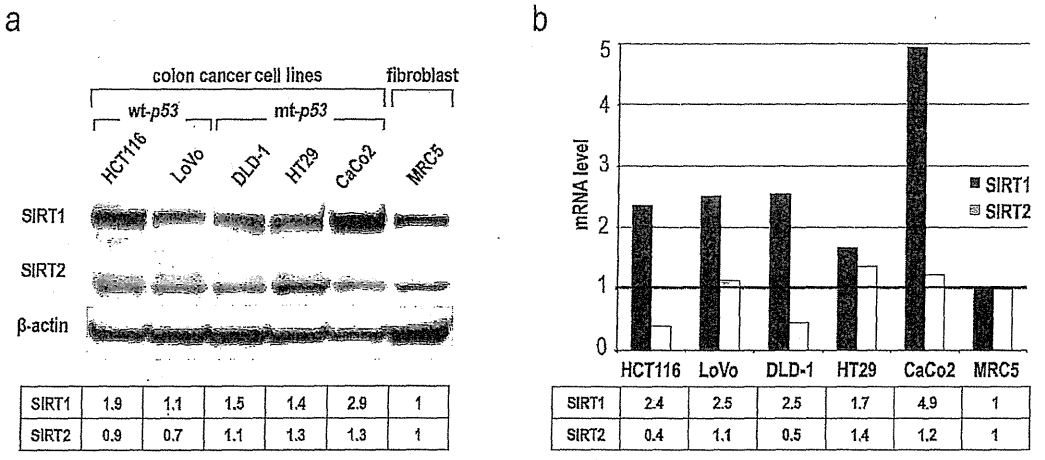

SIRT1	1.9	1.1	1.5	1.4	2.9	1
SIRT2	0.9	0.7	1.1	1.3	1.3	1

SIRT1	2.4	2.5	2.5	1.7	4.9	1
SIRT2	0.4	1.1	0.5	1.4	1.2	1

Figure 2. Expression levels of SIRT1 and SIRT2 in colon cancer cell lines. (a) The expression of SIRT1 and SIRT2 in five colon cancer cell lines and normal fibroblasts (MRC5) was examined by Western blotting. Quantification of Western blot densitometry involved normalization to β-actin levels. (b) *SIRT1* and *SIRT2* mRNA levels in five colon cancer cell lines and MRC5 cells were analyzed by quantitative real-time PCR.

Next, we compared sensitivity to tenovin-6 between colon cancer cells and control cells (Fig. 3b). At a concentration of 2 and 5 μM, cell viability of MRC5 cells as a normal control was significantly higher than that of HCT116 and DLD-1 colon cancer cells, suggesting that normal fibroblasts were less sensitive to tenovin-6.

To determine whether tenovin-6 causes apoptotic cell death, HCT116 and DLD-1 cells were incubated with 10 μM tenovin-6 for 72 h, double-stained with FITC–annexin V and PI, and analyzed by flow cytometry (Fig. 3c). Cells negative for both annexin V and PI were considered nonapoptotic, those positive for annexin V were considered early apoptotic, and those positive for both annexin V and PI were considered late apoptotic or necrotic. Exposure of HCT116 and DLD-1 cells to tenovin-6 increased the fraction of apoptotic cells from 1.8% to 39.9% and from 11.3% to 50.3%, respectively.

The proteins extracted from the five colon cancer cell lines treated with 10 μM tenovin-6 for 0, 4, 8, and 24 h were analyzed by Western blotting (Fig. 3d). In the cells carrying wt-*p53* (HCT116 and LoVo), tenovin-6 increased p53 expression in a time-dependent manner, but this effect was weak or nonexistent in cell lines carrying mt-*p53* (DLD-1, HT29, and CaCo2). Upregulation of $p21^{Waf/Cip1}$ was observed only in cells with wt-*p53* (HCT116 and LoVo) in response to tenovin-6 exposure. Acetylation of p53 was observed in HCT116 cells but not in LoVo cells.

We found that DR5 was strongly upregulated after tenovin-6 administration in all colon cancer cell lines except for CaCo2. Cleaved PARP was observed in the four cell lines that accumulated DR5 in response to tenovin-6. Upregulation of DR5 and cleaved PARP were independent of the *p53* mutation status.

Activation of the Apoptotic Pathway by Tenovin-6 Was Attenuated by DR5 Silencing

We tested whether tenovin-6-induced cell death was inhibited by DR5 knockdown. HCT116 cells were transfected with DR5 siRNA (1 nM) or control siRNA (1 nM) for 48 h, and 10 μM tenovin-6 or DMSO only was administered for 24 h. Total cell protein was extracted to analyze the expression levels of DR5, cleaved PARP, and cleaved caspase-3 in mock-, control siRNA- or DR5 siRNA-transfected HCT116 cells. DR5 knockdown HCT116 cells expressed less of the proapoptotic proteins (cleaved PARP and cleaved caspase-3) after tenovin-6 administration compared with the control (Fig. 4a). HCT116 cells transfected with DR5 siRNA (1 nM) or control siRNA (1 nM) for 48 h were exposed to tenovin-6 at concentrations of 0, 0.2, 1, and 5 μM. Cell viability was determined 72 h later. Inhibition of DR5 expression by specific siRNA significantly reduced tenovin-6-induced cell death in HCT116 cells (Fig. 4b).

Antitumor Effects of Tenovin-6 in Combination With Cytotoxic Drugs

We examined the combined effects of tenovin-6 and cytotoxic agents such as oxaliplatin, 5-FU, or SN-38 on cell viability. HCT116 (wt-*p53*) and DLD-1 (mt-*p53*) cells were exposed either to a single agent or to combinations (tenovin-6 plus oxaliplatin, tenovin-6 plus 5-FU, and tenovin-6 plus SN-38) for 72 h and tested for viability. As shown in Table 1, tenovin-6 combined with either

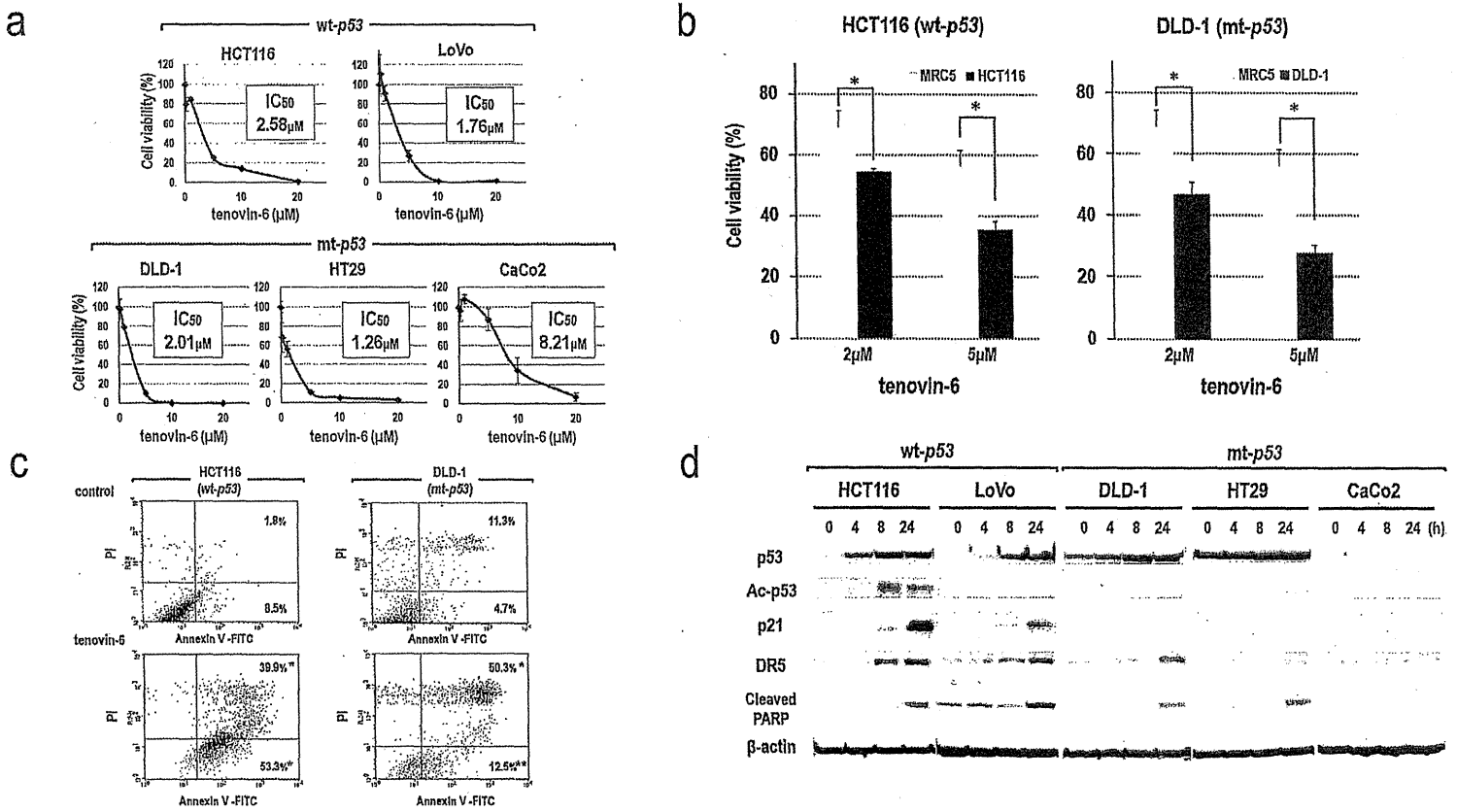

Figure 3. Tenovin-6 induced apoptosis in colon cancer cells. (a) Five colon cancer cell lines were treated with increasing doses of tenovin-6 for 72 h. Cell growth was assessed by the WST-8 assay. Tenovin-6 strongly inhibited the growth of colon cancer cells regardless of the *p53* status. All experiments were performed in triplicate, and the results are expressed as the mean ± SD. (b) HCT116 and DLD-1 cells and MRC5 fibroblasts were treated with 2 and 5 μM tenovin-6 for 72 h. Tenovin-6 inhibited colon cancer cell growth more effectively compared with control (MRC5) cells. $*p<0.01$. (c) HCT116 and DLD-1 were treated with 10 μM tenovin-6 for 72 h. Apoptotic cells were analyzed by PI–annexin V staining and flow cytometry. $*p<0.01$, $**p<0.05$. (d) Effects of tenovin-6 on the expression of p53, acetylated p53, regular p21, DR5, and cleaved PARP were analyzed by Western blotting. The five colon cancer cell lines were treated with 10 μM tenovin-6 for 0, 4, 8, and 24 h.

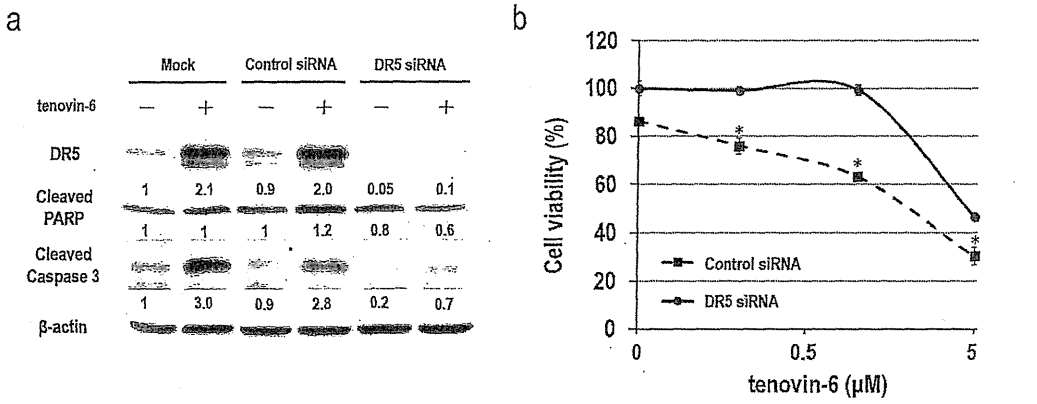

Figure 4. DR5 silencing attenuated the antitumor effect of tenovin-6. (a) HCT116 cells were transfected with DR5 siRNA (1 nM) or control siRNA (1 nM) for 48 h and then either tenovin-6 or DMSO (vehicle) was administered. After 24 h, the protein expression levels of DR5, cleaved PARP, and cleaved caspase-3 were assessed by Western blotting. Quantification of Western blot densitometry involved normalization to β-actin levels. DR5 knockdown HCT116 cells expressed less of the apoptotic proteins (cleaved PARP and cleaved caspase 3) after tenovin-6 administration than the control. (b) HCT116 cells were transfected with DR5 siRNA (1 nM) or control siRNA (1 nM) for 48 h and then treated with 10 μM tenovin-6. Cell viability was determined after 72 h incubation. All experiments were carried out in triplicate, and the results are expressed as the mean ± SD. $^*p<0.01$. Inhibition of DR5 expression by specific siRNA significantly reduced tenovin-6-induced cell death in HCT116 cells.

oxaliplatin or 5-FU showed synergistic effects in both cell lines. Tenovin-6 combined with oxaliplatin strongly induced DR5 in HCT116 cells (Fig. 5).

In Vivo Antitumor Effects of Tenovin-6 Alone or in Combination With Oxaliplatin

These effects were analyzed in a HCT116 xenograft tumor model based on nude mice (immunosuppressed animals). In the group receiving tenovin-6 alone, one mouse died on day 16, with weight loss. Except for this adverse event, all mice tolerated tenovin-6 treatment well (30 mg/kg), and the same was true of oxaliplatin (alone or in combination, 5 mg/kg). The combination of tenovin-6 and oxaliplatin significantly inhibited the growth of xenograft tumors compared with the control (Fig. 6).

DISCUSSION

Earlier studies have suggested that p53 plays an important role in the antitumor effect of tenovin-6, the main mechanism of which is dependent on p53 activation (17,18). This notion seems to contradict our present results, since the tenovin-6-induced antitumor effect did not depend on the status of *p53* as colon cancer cells harboring wt-*p53* and those harboring mt-*p53* were both sensitive to tenovin-6, with IC_{50} values in the single-digit micromolar range. These data indicate that the antitumor effect of tenovin-6 is mediated by additional pathways. We found that tenovin-6 strongly upregulates DR5 expression in colon cancer cells. Our data show that a knockdown of *DR5* by siRNA in HCT116 cells attenuates the antitumor effect of tenovin-6. These results suggest that tenovin-6 induces death receptor signaling through DR5, leading to apoptosis. CaCo2 cells, which do not strongly upregulate DR5 expression in response to tenovin-6 exposure, are less sensitive to tenovin-6 than the other four colon cancer cell lines, according to our results. This observation supports our supposition that tenovin-6 exerts its antitumor effect via DR5 rather than p53 activation.

Recent reports have demonstrated that heat shock protein 70 (HSP70), known as one of molecular chaperones,

Table 1. The Combination Index (CI) of Tenovin-6 and Cytotoxic Agents [Oxaliplatin, 5-Fluorouracil (5-FU), or SN-38] in HCT116 and DLD-1 Cells

		Combination Index	
		HCT116	DLD-1
Tenovin-6: 2 μM	oxaliplatin: 2 μM	***0.691***	0.976
Tenovin-6: 5 μM	oxaliplatin: 2 μM	***0.659***	***0.829***
Tenovin-6: 2 μM	5-FU: 2 μM	***0.847***	***0.837***
Tenovin-6: 5 μM	5-FU: 2 μM	***0.639***	***0.853***
Tenovin-6: 2 μM	SN-38: 2 nM	1.189	n/a
Tenovin-6: 5 μM	SN-38: 2 nM	1.282	n/a

CI > 1.3, antagonistic; CI = 1.1–1.3, moderately antagonistic; CI = 0.9–1.1, additive; CI = 0.8–0.9, slightly synergistic; CI = 0.6–0.8, moderately synergistic; CI = 0.4–0.6 synergistic; and CI = 0.2–0.4, strongly synergistic effects. n/a (not available). Bold and italic numbers indicate synergistic effects.

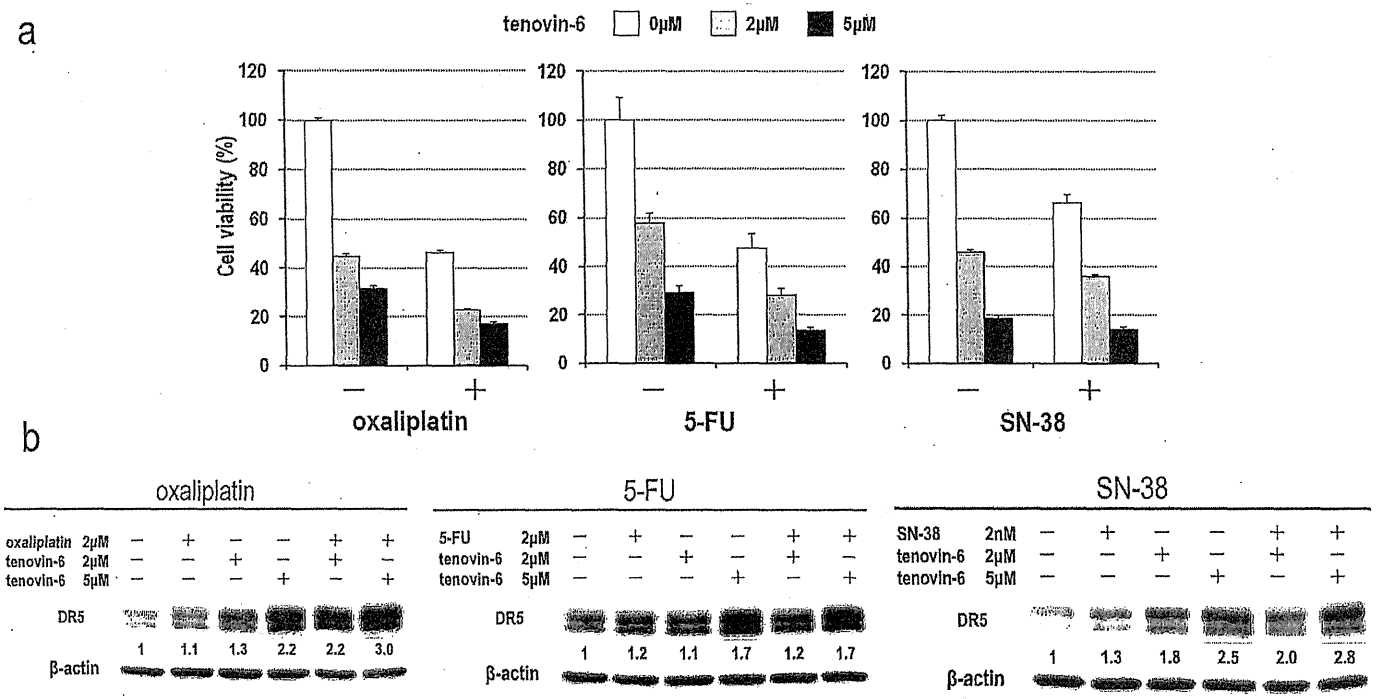

Figure 5. Antitumor effects of tenovin-6 in combination with cytotoxic drugs. (a) HCT116 cells were treated with tenovin-6 and/or cytotoxic drugs (oxaliplatin, 5-FU, or SN-38) for 72 h. All experiments were carried out in triplicate, and the results are expressed as the mean±SD. (b) After treatment with tenovin-6 and/or cytotoxic drugs for 8 h, DR5 expression in HCT116 cells was analyzed by Western blotting. Quantification of Western blot densitometry involved normalization to β-actin levels.

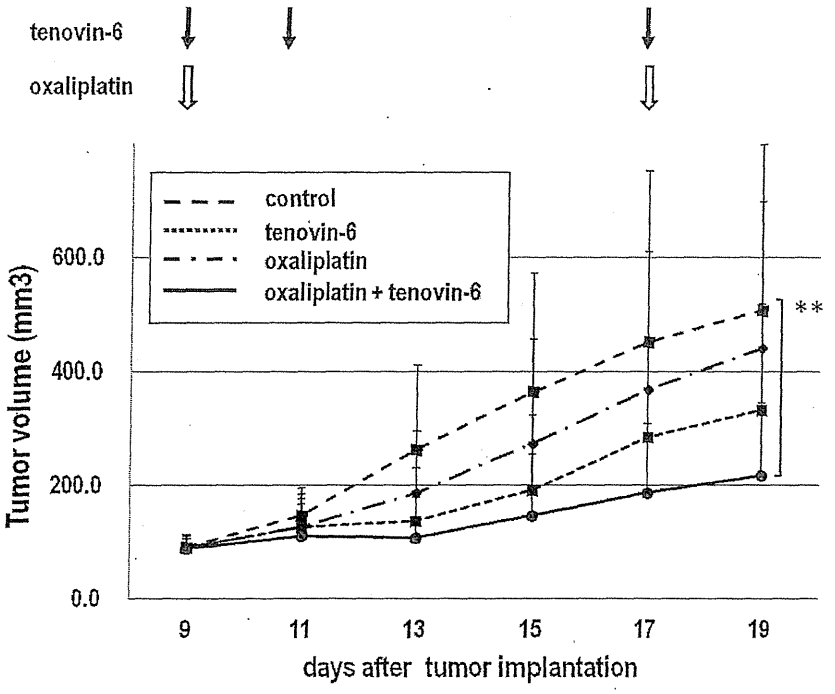

Figure 6. In vivo antitumor effects of tenovin-6. Antitumor effects of tenovin-6 alone and in combination with oxaliplatin in a mouse xenograft model, where HCT116 cells were injected (vehicle, $n=6$; oxaliplatin, $n=6$; tenovin-6, $n=5$; and oxaliplatin plus tenovin-6, $n=6$). Drugs administered intraperitoneally are indicated by arrows at the top of the graph. On day 19, the average estimated xenograft volume of the group receiving tenovin-6 plus oxaliplatin was less than half of that in the control group. The results are expressed as the mean±SD. $^{**}p<0.05$.

suppresses DR5 expression and regulates apoptosis at various points in the death receptor signaling pathway (30,31). Some earlier studies showed that CaCo2 cells constitutively express high levels of heat shock proteins (32,33). These observations may explain why tenovin-6-induced apoptotic cell death is less evident in CaCo2 cells in our experiments.

DR5 expression is known to be induced without ligand–receptor interactions during cellular stress. We did not detect upregulation of TRAIL proteins in colon cancer cells treated with tenovin-6 in our experiments (data not shown). This ligand-independent activation of DR5 mediated by tenovin-6 would result in the activation of the extrinsic apoptosis pathway. Several possible mechanisms of DR5 upregulation by sirtuin inhibitors have been reported. Salermide, another sirtuin inhibitor, also upregulates DR5 in human non-small cell lung cancer (NSCLC) cells, and this effect is accompanied by the accumulation of activating transcription factor 4 (ATF4) and C/EBP homologous protein (CHOP); the latter two proteins are linked to endoplasmic reticulum (ER) stress (34). Reactive oxygen species and c-Jun N-terminal kinase (JNK) have been suggested as players that upregulate the expression of death receptors in NSCLC and pancreatic cancer cells (35,36). Ku70 acetylated by a SIRT1 inhibitor activates the c-Myc/ATF4/CHOP pathway and mediates DR5 induction in HepG2 cells (37). These molecules may contribute to tenovin-6-induced DR5 expression in colon cancer cells as well.

Recently, SIRT2 was reported as an important regulator of programmed necrosis induced by TNF-α. A report shows that DR5 upregulation is strongly induced by silencing of both SIRT1 and SIRT2 in NSCLC cells (34). Nonetheless, the exact role of SIRT2 in cancer biology is poorly understood.

A well-known cytotoxicity mechanism of platinum-based drugs is DNA alkylation (38). HDAC inhibitors induce hyperacetylation of histones and activate the expression of various genes (39). Simultaneously, chromatin becomes more accessible for platinum-based drugs as a result of histone acetylation (40). In addition, platinum-based drugs are known to shift the redox balance toward oxidative stress and induce DNA damage in cancer cells. A HDAC inhibitor suberoylanilide hydroxamic acid (SAHA) has been reported to have an

antitumor effect, possibly by producing oxidative stress and decreasing the ability to combat free radicals via thioredoxin downregulation (41,42). Taking the above mechanisms into account, it appears that HDAC inhibitors have some advantages when used in combination with platinum-based drugs. Indeed, we observed synergistic effects when tenovin-6 and oxaliplatin were used in combination. A recent study showed that oxaliplatin enhances TRAIL-induced apoptosis in gastric cancer cells via death receptor redistribution (43). This phenomenon suggests that TRAIL enhances the antitumor effect of tenovin-6 in combination with oxaliplatin. A synergistic antitumor effect was also reported for the combination of 5-FU with another SIRT1 inhibitor, EX-527 (44). Similar results were obtained in our present study. Combination of SN-38 and tenovin-6 shows antagonistic properties in HCT116 cells in our study, and no other reports have shown the effectiveness of combined treatment of class III HDAC inhibitors and SN-38. The interactions between cytotoxic drugs and sirtuin inhibitors need further research. In conclusion, our data show that tenovin-6 has a robust antitumor effect against human colon cancer cells and acts mostly through the DR5 pathway. This effect appears to be enhanced by oxaliplatin or 5-FU. Our results suggest that a dual SIRT1 and SIRT2 inhibitor holds promise in the treatment of colorectal cancer.

ACKNOWLEDGMENTS: This work was supported in part by grants-in-aid from the Ministry of Education, Culture, Sports, Science, and Technology of Japan (to I.H.).

REFERENCES

1. Vogelstein, B.; Lane, D.; Levine, A. J. Surfing the p53 network. Nature 408:307–310; 2000.
2. Sherr, C. J.; McCormick, F. The RB and p53 pathways in cancer. Cancer Cell 2:103–112; 2002.
3. Feki, A.; Irminger-Finger, I. Mutational spectrum of p53 mutations in primary breast and ovarian tumors. Crit. Rev. Oncol. Hematol. 52:103–116; 2004.
4. Inoue, T.; Hiratsuka, M.; Osaki, M.; Oshimura, M. The molecular biology of mammalian SIRT proteins: SIRT2 in cell cycle regulation. Cell Cycle 6:1011–1018; 2007.
5. Guarente, L.; Franklin, H. Epstein Lecture: Sirtuins, aging, and medicine. N. Engl. J. Med. 364:2235–2244; 2011.
6. Donmez, G.; Guarente, L. Aging and disease: Connections to sirtuins. Aging Cell 9:285–290; 2010.
7. Carafa, V.; Nebbioso, A.; Altucci, L. Sirtuins and disease: The road ahead. Front. Pharmacol. 3:4; 2012.
8. Liu, T.; Liu, P. Y.; Marshall, G. M. The critical role of the class III histone deacetylase SIRT1 in cancer. Cancer Res. 69:1702–1705; 2009.
9. Olmos, Y.; Brosens, J. J.; Lam, E. W. Interplay between SIRT proteins and tumour suppressor transcription factors in chemotherapeutic resistance of cancer. Drug Resist. Updat. 14:35–44; 2011.
10. Kruse, J. P.; Gu, W. Modes of p53 regulation. Cell 137:609–622; 2009.
11. Kim, J. H.; Yoon, E. K.; Chung, H. J.; Park, S. Y.; Hong, K. M.; Lee, C. H.; Lee, Y. S.; Choi, K.; Yang, Y.; Kim, K.; Kim, I. H. p53 acetylation enhances Taxol-induced apoptosis in human cancer cells. Apoptosis 18:110–120; 2013.
12. Nosho, K.; Shima, K.; Irahara, N.; Kure, S.; Firestein, R.; Baba, Y.; Toyoda, S.; Chen, L.; Hazra, A.; Giovannucci, E. L.; Fuchs, C. S.; Ogino, S. SIRT1 histone deacetylase expression is associated with microsatellite instability and CpG island methylator phenotype in colorectal cancer. Mod. Pathol. 22:922–932; 2009.
13. Cha, E. J.; Noh, S. J.; Kwon, K. S.; Kim, C. Y.; Park, B. H.; Park, H. S.; Lee, H.; Chung, M. J.; Kang, M. J.; Lee, D. G.; Moon, W. S.; Jang, K. Y. Expression of DBC1 and SIRT1 is associated with poor prognosis of gastric carcinoma. Clin. Cancer Res. 15:4453–4459; 2009.
14. Portmann, S.; Fahrner, R.; Lechleiter, A.; Keogh, A.; Overney, S.; Laemmle, A.; Mikami, K.; Montani, M.; Tschan, M. P.; Candinas, D.; Stroka, D. Antitumor effect of SIRT1 inhibition in human HCC tumor models in vitro and in vivo. Mol. Cancer Ther. 12:499–508; 2013.
15. Narayan, N.; Lee, I. H.; Borenstein, R.; Sun, J. H.; Wong, R.; Tong, G.; Fergusson, M. M.; Liu, J.; Rovira, I. I.; Cheng, H. L.; Wang, G. H.; Gucek, M.; et al. The NAD-dependent deacetylase SIRT2 is required for programmed necrosis. Nature 492:199–204; 2012.
16. Hammond, J. W.; Cai, D. W.; Verhey, K. J. Tubulin modifications and their cellular functions. Curr. Opin. Cell Biol. 20:71–76; 2008.
17. Brooks, C. L.; Gu, W. p53 Activation: A case against Sir. Cancer Cell 13:377–378; 2008.
18. Lain, S.; Hollick, J. J.; Campbell, J.; Staples, O. D.; Higgins, M.; Aoubala, M.; McCarthy, A.; Appleyard, V.; Murray, K. E.; Baker, L.; Thompson, A.; Mathers, J.; et al. Discovery, in vivo activity, and mechanism of action of a small-molecule p53 activator. Cancer Cell 13:454–463; 2008.
19. Alcain, F. J.; Villalba, J. M. Sirtuin inhibitors. Expert Opin. Ther. Pat. 19:283–294; 2009.
20. McCarthy, A. R.; Pirrie, L.; Hollick, J. J.; Ronseaux, S.; Campbell, J.; Higgins, M.; Staples, O. D.; Tran, F.; Slawin, A. M.; Lain, S.; Westwood, N. J. Synthesis and biological characterisation of sirtuin inhibitors based on the tenovins. Bioorg. Med. Chem. 20:1779–1793; 2012.
21. Singh, T. R.; Shankar, S.; Srivastava, R. K. HDAC inhibitors enhance the apoptosis-inducing potential of TRAIL in breast carcinoma. Oncogene 24:4609–4623; 2005.
22. Kim, Y. H.; Park, J. W.; Lee, J. Y.; Kwon, T. K. Sodium butyrate sensitizes TRAIL-mediated apoptosis by induction of transcription from the DR5 gene promoter through Sp1 sites in colon cancer cells. Carcinogenesis 25:1813–1820; 2004.
23. Nakata, S.; Yoshida, T.; Horinaka, M.; Shiraishi, T.; Wakada, M.; Sakai, T. Histone deacetylase inhibitors upregulate death receptor 5/TRAIL-R2 and sensitize apoptosis induced by TRAIL/APO2-L in human malignant tumor cells. Oncogene 23:6261–6271; 2004.
24. VanOosten, R. L.; Moore, J. M.; Karacay, B.; Griffith, T. S. Histone deacetylase inhibitors modulate renal cell carcinoma sensitivity to TRAIL/Apo-2L-induced apoptosis by enhancing TRAIL-R2 expression. Cancer Biol. Ther. 4:1104–1112; 2005.
25. Earel, J. K., Jr.; VanOosten, R. L.; Griffith, T. S. Histone deacetylase inhibitors modulate the sensitivity of tumor necrosis factor-related apoptosis-inducing ligand-resistant bladder tumor cells. Cancer Res. 66:499–507; 2006.
26. Fulda, S. Histone deacetylase (HDAC) inhibitors and regulation of TRAIL-induced apoptosis. Exp. Cell Res. 318:1208–1212; 2012.

27. Endo, S.; Yamato, K.; Hirai, S.; Moriwaki, T.; Fukuda, K.; Suzuki, H.; Abei, M.; Nakagawa, I.; Hyodo, I. Potent in vitro and in vivo antitumor effects of MDM2 inhibitor nutlin-3 in gastric cancer cells. Cancer Sci. 102:605–613; 2011.
28. Yamato, K.; Yamada, T.; Kizaki, M.; Ui-Tei, K.; Natori, Y.; Fujino, M.; Nishihara, T.; Ikeda, Y.; Nasu, Y.; Saigo, K.; Yoshinouchi, M. New highly potent and specific E6 and E7 siRNAs for treatment of HPV16 positive cervical cancer. Cancer Gene Ther. 15:140–153; 2008.
29. Chou, T. C.; Talalay, P. Quantitative analysis of dose-effect relationships: The combined effects of multiple drugs or enzyme inhibitors. Adv. Enzyme Regul. 22:27–55; 1984.
30. Goloudina, A. R.; Demidov, O. N.; Garrido, C. Inhibition of HSP70: A challenging anti-cancer strategy. Cancer Lett. 325:117–124; 2012.
31. Guo, F.; Sigua, C.; Bali, P.; George, P.; Fiskus, W.; Scuto, A.; Annavarapu, S.; Mouttaki, A.; Sondarva, G.; Wei, S.; Wu, J.; Djeu, J.; et al. Mechanistic role of heat shock protein 70 in Bcr-Abl-mediated resistance to apoptosis in human acute leukemia cells. Blood 105:1246–1255; 2005.
32. Musch, M. W.; Kaplan, B.; Chang, E. B. Role of increased basal expression of heat shock protein 72 in colonic epithelial c2BBE adenocarcinoma cells. Cell Growth Differ. 12:419–426; 2001.
33. Malago, J. J.; Koninkx, J. F.; Ovelgonne, H. H.; van Asten, F. J.; Swennenhuis, J. F.; van Dijk, J. E. Expression levels of heat shock proteins in enterocyte-like Caco-2 cells after exposure to Salmonella enteritidis. Cell Stress Chaperones 8:194–203; 2003.
34. Liu, G.; Su, L.; Hao, X.; Zhong, N.; Zhong, D.; Singhal, S.; Liu, X. Salermide up-regulates death receptor 5 expression through the ATF4-ATF3-CHOP axis and leads to apoptosis in human cancer cells. J. Cell. Mol. Med. 16:1618–1628; 2012.
35. Zou, W.; Liu, X.; Yue, P.; Zhou, Z.; Sporn, M. B.; Lotan, R.; Khuri, F. R.; Sun, S. Y. c-Jun NH2-terminal kinase-mediated up-regulation of death receptor 5 contributes to induction of apoptosis by the novel synthetic triterpenoid methyl-2-cyano-3,12-dioxooleana-1, 9-dien-28-oate in human lung cancer cells. Cancer Res. 64:7570–7578; 2004.
36. Kong, R.; Jia, G.; Cheng, Z. X.; Wang, Y. W.; Mu, M.; Wang, S. J.; Pan, S. H.; Gao, Y.; Jiang, H. C.; Dong, D. L.; Sun, B. Dihydroartemisinin enhances Apo2L/TRAIL-mediated apoptosis in pancreatic cancer cells via ROS-mediated up-regulation of death receptor 5. PLoS One 7:e37222; 2012.
37. Kim, M. J.; Hong, K. S.; Kim, H. B.; Lee, S. H.; Bae, J. H.; Kim, D. W.; Dao, T. T.; Oh, W. K.; Kang, C. D.; Kim, S. H. Ku70 acetylation and modulation of c-Myc/ATF4/CHOP signaling axis by SIRT1 inhibition lead to sensitization of HepG2 cells to TRAIL through induction of DR5 and down-regulation of c-FLIP. Int. J. Biochem. Cell Biol. 45:711–723; 2013.
38. Olszewski, U.; Hamilton, G. A better platinum-based anticancer drug yet to come? Anticancer Agents Med. Chem. 10:293–301; 2010.
39. de Ruijter, A. J.; van Gennip, A. H.; Caron, H. N.; Kemp, S.; van Kuilenburg, A. B. Histone deacetylases (HDACs): Characterization of the classical HDAC family. Biochem. J. 370:737–749; 2003.
40. Diyabalanage, H. V.; Granda, M. L.; Hooker, J. M. Combination therapy: Histone deacetylase inhibitors and platinum-based chemotherapeutics for cancer. Cancer Lett. 329:1–8; 2013.
41. Butler, L. M.; Zhou, X.; Xu, W. S.; Scher, H. I.; Rifkind, R. A.; Marks, P. A.; Richon, V. M. The histone deacetylase inhibitor SAHA arrests cancer cell growth, up-regulates thioredoxin-binding protein-2, and down-regulates thioredoxin. Proc. Natl. Acad. Sci. USA 99:11700–11705; 2002.
42. Ruefli, A. A.; Ausserlechner, M. J.; Bernhard, D.; Sutton, V. R.; Tainton, K. M.; Kofler, R.; Smyth, M. J.; Johnstone, R. W. The histone deacetylase inhibitor and chemotherapeutic agent suberoylanilide hydroxamic acid (SAHA) induces a cell-death pathway characterized by cleavage of Bid and production of reactive oxygen species. Proc. Natl. Acad. Sci. USA 98:10833–10838; 2001.
43. Xu, L.; Qu, X.; Zhang, Y.; Hu, X.; Yang, X.; Hou, K.; Teng, Y.; Zhang, J.; Sada, K.; Liu, Y. Oxaliplatin enhances TRAIL-induced apoptosis in gastric cancer cells by CBL-regulated death receptor redistribution in lipid rafts. FEBS Lett. 583:943–948; 2009.
44. Kabra, N.; Li, Z. Y.; Chen, L. H.; Li, B. Z.; Zhang, X. H.; Wang, C. G.; Yeatman, T.; Coppola, D.; Chen, J. D. SirT1 is an inhibitor of proliferation and tumor formation in colon cancer. J. Biol. Chem. 284:18210–18217; 2009.